UNIVERSITÉ DE MONTRÉAL

CONVECTION OF WATER NEAR 4 °C IN AN ANISOTROPIC POROUS MEDIUM

WEI ZHENG

DÉPARTEMENT DE GÉNIE MÉCANIQUE

ÉCOLE POLYTECHNIQUE DE MONTRÉAL

MÉMOIRE PRÉSENTÉ EN VUE DE L'OBTENTION

DU DIPLÔME DE MAÎTRISE ÈS SCIENCES APPLIQUÉES

(GÉNIE MÉCANIQUE)

NOVEMBER 2000

UNIVERSITÉ DE MONTRÉAL

ÉCOLE POLYTECHNIQUE DE MONTRÉAL

Ce mémoire intitulé:

CONVECTION OF WATER NEAR 4 °C IN AN ANISOTROPIC POROUS MEDIUM

présenté par: WEI Zheng

en vue de l'obtention du diplôme de: Maîtrise ès sciences appliquées

a été dûment accepté par le jury d'examen constitué de:

M. PARASCHIVOIU Ion, Ph.D., président

M. VASSEUR Patrick, Ph.D., directeur de recherche

M. ROBILLARD Luc, D.Sc., codirecteur de recherche

M. PRUD'HOMME Michel, Ph. D., membre

Dedicated to my wife, my son and my parents

ACKNOWLEDGEMENTS

First of all, I would like to express my great appreciation to my supervisors, professors Patrick Vasseur, and Luc Robillard for their encouragement and guidance in all phases of my graduate studies in the Department of Mechanical Engineering, Ecole Polytechnique. It was a great pleasure to study and work under their supervision, and I have gained a lot from my discussions with them on my research project. Their profound interpretation of the physical phenomenon and ingenuity in doing scientific research will considerably influence my future life of study and research.

It is also a good chance for me to thank my professors, staff, fellow graduate students and friends in the department for their help in various forms.

RÉSUMÉ

La convection naturelle de l'eau au voisinage de 4 °C est un phénomène important à cause de ses nombreuses applications dans le domaine de la technologie et du génie. La présente étude est limitée au cas de la convection confinée au sein d'une cavité rectangulaire.

Au début de la thèse, les études antérieures portant sur ce sujet sont passées en revue. Tout d'abord, le problème de l'inversion de densité dans des milieux poreux et fluides est discuté. Ensuite, on considère les travaux disponibles sur les milieux poreux anisotropiques.

Le modèle physique pour l'écoulement de l'eau dans un milieu anisotropique est développé sur la base de la loi de Darcy et de l'approximation de Boussinesq. Les paramètres gouvernant le présent problème sont le nombre de Rayleigh Ra_m, le paramètre d'inversion de densité γ, le rapport d'anisotropie K^*, l'angle d'orientation θ, le rapport de forme de la cavité A et l'inclinaison de la cavité ϕ. Une méthode numérique basée sur les différences finies est proposée pour résoudre les équations de base gouvernant le présent problème.

Le cas d'une cavité verticale est d'abord considéré. Les parois horizontales sont maintenues adiabatiques alors que les parois verticales sont isothermes. Les effets du paramètre d'inversion de densité γ sont étudiés pour le cas où les paramètres θ, K^* et Ra_m sont maintenus constants. Les champs d'écoulement montrent que lorsque γ est accru de 0 à 100, la présence d'une cellule de convection tournant initialement dans le sens des aiguilles d'une montre est progressivement remplacée par une cellule tournant dans le sens contraire. Dans le cas spécial où $\gamma = 1$, deux cellules symétriques existent

dans la cavité. Lorsque γ augmente, la cellule originale disparaît progressivement et le nombre de Nusselt s'accroît.

Les effets du paramètre K^* sur les champs d'écoulement et de température sont également étudiés. Au fur et à mesure que la valeur de K^* augmente de 10^{-2} à 10^2, on observe que l'écoulement et le transfert de chaleur sont progressivement accrus.

Finalement, les effets de l'angle d'orientation de l'anisotropie θ sont étudiés. Les résultats indiquent que pour $\gamma=1$, l'écoulement consiste en deux cellules de convection symétriques quand $\theta=0^o$ et 90^o. Pour les autres valeurs de θ, l'écoulement est alors non sysmétrique.

Dans le dernier chapitre, on présente les conclusions de cette étude et des recommandations pour des études futures sont faites.

ABSTRACT

Natural convection of water near 4 $^{\circ}C$ in an anisotropic porous medium is an important topic because of its various applications in the contemporary science, technology and engineering activities. The present study is focusing on convection confined in a rectangular cavity.

At the beginning of the thesis, the previous existing studies on this subject are carefully reviewed. First, the problem of the inversion of density is discussed, and then the topic of natural convection in an anisotropic porous medium is considered.

The flow model in the present study, based on Darcy's law and Boussinesq approximation is first presented. The governing parameters of the model are the Rayleigh number Ra_m, the density inversion parameter γ, the anisotropic ratio K^*, and the anisotropic orientation angle θ combined with the cavity aspect ratio A and the inclination angle ϕ introduced into the flow model. The numerical solution makes it possible to investigate the convection in a rectangular cavity for different combination of these parameters. The numerical approach based on the finite difference method for the present flow model is presented in the following chapter. ADI and SOR methods are used here to perform the numerical calculation.

Some results and discussions for the case of a vertical cavity with adiabatic horizontal walls and isotherm vertical walls are presented in Chapter 3 of the thesis. The effects of the inversion density parameter γ are investigated when the orientation angle θ, anisotropic ratio K^* and Rayleigh number Ra_m are maintained constant. The flow fields show that, when γ is increasing from 0 to 10, the original clockwise cell is gradually replaced by a counterclockwise cell which appears first near the right wall. With γ increasing, this cell is enhanced to produce two symmetrical cells when $\gamma = 1$.

As γ increases further, the original clockwise cell is reduced in size and strength and is finally eliminated from the flow field. The Nusselt number Nu is enhanced as γ increases.

The effects of K^* are then investigated. The flow and temperature fields show that the distortion of the isotherms, the strength of the flow field and the heat transfer are enhanced with K^* increasing from 0.1 to 100.

At last the effects of anisotropic orientation angle θ, varying from 0° to 90° are studied for the inversion parameter γ=1, anisotropic ratio K^*=0.1, and the Rayleigh number Ra_m=800. The flow and temperature fields show that, when θ=0°, there are two symmetric convection cells located in the flow domain. With θ increasing, the cells become asymmetric in the flow domain and symmetric again at an angle equal to 90°. The Nu number is continuously increasing from its minimum value to its maximum value, with θ increasing from 0° to 90°.

At the end of the thesis, a conclusion is given with some recommendations for the future researches to be done on the subject.

CONDENSÉ EN FRANÇAIS

Introduction

De nombreuses recherches ont été effectuées au cours des années passées pour étudier les mouvements convectifs et l'accroissement du transfert de chaleur qui en résulte dans les cavités contenant un milieu poreux saturé. Ces recherches étaient motivées par les multiples situations pratiques où ces phénomènes se rencontrent, comme celles relevant des technologies modernes, par exemple, l'isolation thermique ou comme celles relevant de l'environement, par exemple, les écoulements dans les sols. La majorité des études a porté sur des milieux poreux isotropes. Cependant, il existe beaucoup de situations pratiques où le milieu poreux est anisotrope, tant au point de vue de la résistance qu'il offre à l'écoulement que de celui des propriétés thermiques.

Il existe un autre aspect particulier, celui qui concerne la relation entre la masse volumique (densité) et la température. Dans la plupart des études effectuées, on considère que la densité est reliée linéairement à la température, ce qui constitue une hypothèse réaliste dans bon nombre d'applications. Cependant, la convection naturelle impliquant l'eau à basse température, c'est-à-dire au voisinage du point de congélation, nécessite une relation non linéaire, au moins du deuxième ordre (parabolique), puisque l'eau possède un maximum de densité à 4 °C. Cette propriété de l'eau entraîne des mouvements convectifs particuliers que l'on appelle mouvements convectifs avec "inversion de densité".

Cette forme de convection où la densité passe par un maximum avec la diminution ou l'augmentation de température a reçu beaucoup moins d'attention de la part des thermiciens malgré le fait qu'elle survient couramment dans les régions nordiques comme le Canada et qu'elle constitue un facteur important dans la formation ou la suppression de la glace dans les cours d'eau, les lacs et les étangs. Au voisinage de

4 °C, les mouvements convectifs ont une allure particulière, ainsi que le démontrent les études sur le sujet. Ces études ont d'abord porté sur le milieu fluide, ensuite sur le milieu poreux isotrope saturé d'eau. Cependant, le milieu anisotrope n'a à peu près pas été considéré.

Le présent travail a pour objectif de préciser la nature des mouvements convectifs en milieu poreux anisotrope saturé d'eau dont la température se situe au voisinage de 4°C. Le domaine physique considéré est celui d'une enceinte de forme rectangulaire chauffée par les côtés. Ou utilisera une modélisation de Darcy généralisée et on considérera la forme non linéaire la plus simple c'est-à-dire la forme parabolique pour relier la densité à la température. Comme on a affaire à des équations couplées dont une (l'équation d'énergie) non linéaire, une approche analytique demeure problématique et par conséquent, nous nous limiterons à une approche numérique.

Modèle mathématique

Le modèle physique faisant l'objet de ce mémoire est montré à la figure1.1. Il s'agit d'une cavité rectangulaire contenant un milieu poreux anisotrope en perméabilité et saturé par de l'eau dont la température se situe au voisinage de 4 °C. La cavité a une hauteur H' et une largeur W'. Elle est inclinée à un angle ϕ par rapport au plan horizontal. Les perméabilités extrêmes le long des axes principaux sont K_1 et K_2, et le rapport d'anisotropie est défini par $K^* = K_2 / K_1$. L'angle d'orientation θ est l'angle entre l'axe x (ce dernier étant parallèle aux côtés de largeur W') et l'axe principal corespondant à K_1. Pour $\phi = 0$, les parois de dimension W' deviennent horizontales et sont considérées adiabatiques. Les parois verticales de gauche et de droite sont maintenues à des températures uniformes respectives T_l' et T_r'.

Le mouvement du fluide à l'intérieur du milieu poreux obéit à la loi de Darcy généralisée pour un milieu anisotrope. On considère qu'il y a équilibre thermodynamique

entre le fluide saturant et la matrice solide, c'est-à-dire que localement, les deux milieux ont la même température. On considère que l'hypothèse de Boussinesq s'applique, de sorte que les propriétés autres que la masse volumique dans le terme de poussée sont considérées constantes. On suppose que la masse volumique varie avec la température selon une relation parabolique. Ce type de relation, la plus simple pour simuler un extremum de masse volumique, a été utilisé dans le passé par différents auteurs.

Les équations exprimant la conservation de la masse, de la quantité de mouvement et de l'énergie sont à la base du présent problème et sont réduites à l'équation de fonction de courant et à l'équation d'énergie en introduisant la définition de la fonction au courant. L'équation de fonction de courant comporte des termes additionnels affectés de coefficients qui proviennent du tenseur de perméabilité. On exprime ces équations sous forme adimensionnelle par l'emploi de facteurs d'échelle appropriés. Il en résulte des paramètres de contrôle qui sont à la base du présent problème. Ces paramètres sont le nombre de Rayleigh non linéaire, Ra, le paramètre d'inversion, γ, le rapport de perméabilité, $K^* = K_2 / K_1$, l'angle d'orientation des axes principaux par rapport à la cavité, θ, l'angle d'inclinaison de la cavité, ϕ, et finalement le rapport de forme $A = W' / H'$.

Si la paramètre d'inversion prend des valeurs importantes, le problème considéré rejoint le cas classique d'une masse volumique reliée linéairement à la température. D'autre part, si le rapport d'anisotropie K^* devient égal à l'unité, le modèle actuel devient celui d'un milieu isotrope.

Il convient de signaler que l'inverse du tenseur de perméabilité $\overline{\overline{K}}$ est appelé le tenseur de résistance hydraulique $\overline{\overline{R}} = (\overline{\overline{K}})^{-1}$, et que $\overline{\overline{R}}$ peut être interprété comme la somme de deux termes, l'un étant la matrice d'identité, valable pour un milieu isotrope, et l'autre, donnant la véritable contribution anisotrope.

Le nombre de Nusselt local correspond au rapport du transfert de chaleur total, convection additionnée à la conduction, divisé par le transfert de chaleur conductif, le tout évalué en un point donné du domaine. Le nombre de Nusselt global est obtenu en intégrant le nombre de Nusselt local sur l'une ou l'autre des deux frontières isothermes.

Approche numérique

Il existe plusieurs techniques pous discrétiser et résoudre les équations de base du présent problème. Parmi ces diverses techniques, l'approche des différence finies est la plus directe, en particulier lorsque la géometrie considérée est simple, comme c'est le cas pour la cavité rectangulaire. C'est l'approche que nous utilisons dans le présent travail. Cette partie donne un aperçu général du rôle et de la nature des techniques numériques relevant de la méthode des différences finies. Une description détaillée du problème numerique telle qu' elle est appliquée au présent problème, applicable également à une variété d'autres problèmes, y est présentée.

Dans l'approche des différences finies, le domaine est discrétisé de telle sorte que les variables dépendantes ne sont considérées qu'aux points de discrétisation. Les dérivées sont approximées par des différences résultant en une représentation algébrique des équations différentielles partielles (PDE). Pour procéder à un calcul numérique, les équations différentielles de base doivent être transformées en des expressions discrètes. Compte tenu du mouvement convectif plutôt lent caractérisant le présent problème, tous les termes diffusifs et convectifs des équations sont discrétisés selon un schéma du deuxième ordre, basé sur une expansion de Taylor; les dérivées temporelles sont discrétisées par des différences avec progression dans le temps. Afin d'accélérer la convergence dans la solution de l'équation de fonction de courant, on utilise une procédure de sur-relaxation (SOR) progressive pour les calculs. La solution de l'équation d'énergie est abordée par le biais d'une méthode implicite aux directions alternées(ADI).

L'approche numérique, telle qu'elle est décrite précédemment, est testée et validée à partir de résultats numériques obtenus par d'autres chercheurs, en particulier, par Degan, G. et Vasseur, P., "Natural Convection in a Vertical Slot Filled with an Anisotropic Porous Medium with Oblique Principal Axes", Numerical Heat Transfer, part A, Vol. 30, pp.397-412, 1996. La présente méthode donne des nombres de Nusselt très près de ceux obtenus par les auteurs, et ce, pour différents nombres de Rayleigh et différents rapports de perméabilité et angles d'inclinaison des axes principaux. En outre, les champs de vitesse et de température, représentés par des lignes de courant et des isotermes respectivement, tels qu'obtenus par la présente approche, reproduisent à peu près intégralement ceux de Degan et Vasseur pour les mêmes conditions.

Résultats numériques et discussion

Des résultats spécifiques pour la cavité avec angle d'inclinaison nul ($\phi = 0$) sont présentés dans cette partie. Les parois adiabatiques sont donc horizontales et les parois isothermes verticales. Les résultats sont limités à ceux d'une cavité carrée (A=1) et on suppose la température de l'eau au voisinage de 4 °C, c'est-à-dire que l'on considère la plage de température pour laquelle le maximum de densité exerce un effet important. Nous verrons dans l'ordre l'effet du paramètre d'inversion, γ, celui du rapport d'anisotropie, K^*, celui de l'angle d'orientation des axes principaux, θ, et finalement l'effect combiné de γ et θ.

Effet du paramètre d'inversion

Si on exclut pour le moment les effets d'anisotropie, on se rend compte que la valeur donnée au paramètre d'inversion modifie grandement le transfert de chaleur et le champ de vitesse, d'une manière comparable aux résultats obtenus pour le cas d'un milieu fluide (voir par exemple les références: Robillard L. et Vasseur, P., "Effect du

maximum de densité sur la convection libre de l'eau dans une cavité fermée", Canadian Journal of Civil Engineering, Vol. 6, No. 4, pp 481-493, 1979; Tong, W. and Kooter, J. N. , "Density Inversion Effect on Transient Natural Convection in a Rectangular Enclosure" Int. J. Heat Mass Transfer, Vol.37, pp 927-938, 1994). La position relative $x_m = 1-\gamma/2$ de l'isotherme correspondant à 4 °C par rapport aux parois verticales modifie grandement le transfert de chaleur lorsque $0 < x_m < 1$, c'est-à-dire lorsque le 4 °C est présent dans le champ de température. Cette réduction atteint son maximum à $x_m = 1/2$ ($\gamma = 1$ et l'isotherme 4 °C est à mi-chemin entre les deux parois verticales). Le champ d'écoulement consiste alors en deux cellules de convection parfaitement symétriques par rapport au plan vertical séparant la cavité en deux parties égales. La circulation dans la cavité est telle que le fluide possède un mouvement descendant le long de ce plan. Le fait d'augmenter ou de diminuer légèrement γ par rapport à l'unité change l'intensité relative des deux cellules de convection. À γ=0 (2), une seule cellule de convection existe dans la cavité dans le sens antihoraire (horaire). Pour un nombre de Rayleigh non linéaire fixé, le nombre de Nusselt porté sur graphique en fonction de γ donne une courbe symétrique par rapport à $\gamma = 1$, avec $Nu(\gamma) = Nu(2-\gamma)$. Pour γ atteignant des valeurs bien au-delà de 2, la situation standard de convection avec relation linéaire entre la densité et la température est atteinte.

Effet de rapport de perméabilité

L'étude de cet effet est effectuée pour un paramètre d'inversion $\gamma = 1$ et pour des axes principaux parallèles et perpendiculaires à la gravité terrestre. Dans ces conditions, quelque que soit la valeur du rapport de perméabilité K^*, on conserve la symétrie du champ d'écoulement décrite précédemment.

Pour isoler l'effet du changement de perméabilité de celui du changement de la résistance hydraulique globale, on définit un nombre de Rayleigh modifié,

$Ra_m = 2Ra/(1+K^*)$, la conséquence de cette redéfinition étant que les perméabilités extrêmes K_1 et K_2 ont un poids équivalent dans ce nouveau nombre de Rayleigh.

Le nombre de Nusselt est porté sur graphique en fonction de K^* pour différents nombres de Rayleigh ($Ra_m = 200, 400, 600, 800$). Il en ressort que l'accroissement relatif de la perméabilité verticale favorise le transfert de chaleur global dans la direction horizontale.

L'effet de K^* sur les champs de vitesse et de température est aussi rapporté pour $Ra_m = 400$ et $\gamma = 1$. On constate que la distortion des isothermes est amplifiée avec K^* augmentant, l'importance de la distortion étant reliée à l'importance du transfert de chaleur. Pour chacun des champs de vitesse et de température, on constate que la symétrie par rapport à un plan vertical séparant la cavité en deux parties égales est toujours préservée.

Effet de l'angle d'orientation θ

Le nombre de Nusselt, Nu, et les valeurs extrêmes de la fonction de courant ψ_{min} et ψ_{max} sont portés sur graphique en fonction de l'angle d'orientation θ pour des nombres de Rayleigh modifiés, Ra_m, de 200, 400 et 800. Pour toutes ces courbes, γ et K^* sont gardés constants à des valeurs respectives de 1 et 0.1. Deux séries de champs d'écoulement et de température correspondant à Ra_m=800 et γ=1 sont reproduites à différentes valeurs de θ allant de 0° à 90° pour des valeurs de rapport d'anisotropie respectives K^*=0.1 et K^*=0.05. On peut observer la transition graduelle pour Nu, de sa valeur minimum à sa valeur maximum, lorsque θ varie de 0° a 90°, c'est-à-dire lorsque l'axe correspondant à la perméabilité maximum passe de l'horizontale à la verticale. Par ailleurs, $|\psi_{min}|$ et ψ_{max} évoluent de la valeur $|\psi_{min}|=\psi_{max}$=6.03 pour θ=0° à

$|\psi_{min}| = \psi_{max} = 14.61$ pour $\theta = 90°$. Cependant entre ces deux valeurs, l'évolution de $|\psi_{min}|$ et ψ_{max} n'est pas la même, de sorte que l'intensité des deux cellules de convection associées diffère pour $0° < \theta < 90°$. Avec θ augmentant de 0° a 90°, $|\psi_{min}|$ décroît d'abord pour atteindre une valeur minimum de 5.5 à $\theta = 13°$, pour le cas $Ra_m = 800$, alors que ψ_{max} augmente continuellement de 0° a 90°. Au-delà de $\theta \approx 13°$, $|\psi_{min}|$ augmente à un taux plus rapide que ψ_{max} de sorte que nous retrouvons l'égalité (sans la symétrie) $|\psi_{min}| = \psi_{max}$ à $\theta \approx 24°$.

La périodicité triviale suivante existe pour un milieu poreux anisotrope:

$$\psi(\theta) = \psi(\theta \pm n\pi), \quad T(\theta) = T(\theta \pm n\pi)$$

avec n=1,2,.... De plus, à $\gamma = 1$, les intensités des cellules de convection de gauche et de droite sont reliées selon

$$\psi_{max}(\theta) = -\psi_{min}(\pi - \theta).$$

De cette dernière relation, il est donc possible de représenter ψ_{min} et ψ_{max} en fonction de θ sur un seul graphique.

Effet combiné de γ et θ

On a déjà relevé le fait que pour un milieu anisotrope, le nombre de Nusselt en fonction de γ atteint une valeur minimum à $\gamma = 1$ et que la courbe obtenue est symétrique. De plus, à $\gamma = 1$, les champs de vitesse et de température sont symétriques. Dans le cas d'un milieu anisotrope, les mêmes symétries sont préservées à la condition

que θ=0° ou θ=90°. Autrement, elles n'existent plus et la valeur minimum de Nusselt est reportée à un endroit différent sur l'abscisse γ.

Conclusion

On a étudié les effets d'inversion de densité caractérisant l'eau au voisinage de 4°C pour le cas d'un milieu poreux anisotrope saturé avec de l'eau. La géometrie considérée était celle d'une cavité carrée avec côtés horizontaux adiabatiques et côtés verticaux maintenus à des températures uniformes. Des solutions ont été obtenues par méthodes numériques aux différences finies, en faisant varier de façon indépendante les différents paramètres de contrôle, à savoir, l'angle d'orientation, θ, le rapport de perméabilité, K^*, le paramètre d'inversion, γ, et le nombre de Rayleigh non linéaire, Ra (ou le nombre de Rayleigh modifié, Ra_m). Il convient de rappeler que le paramètre d'inversion, γ, donne la position horizontale de l'isotherme 4 °C en conduction pure (c'est-à-dire l'emplacement horizontal de la densité maximum) par rapport aux parois verticales.

Lorsque θ=0° et 90°, (axes principaux horizontal et vertical), les résultats obtenus indiquent que la convection maximum et le transfert de chaleur maximum se produisent lorsque la perméabilité maximum est dans la direction verticale. Quand les axes sont obliques ($\theta \neq 0°$ ou 90°), on a constaté que la symétrie des champs de vitesse et de température observée pour le cas isotrope à γ=1 (valeur ou les températures des parois verticales sont équidistantes de 4 °C) n'existe plus pour le cas anisotrope. De plus, dans ces conditions, le nombre de Nusselt minimum n'est plus à γ=1, mais est déplacé à une valeur légèrement différente, plus haute ou plus basse.

TABLE OF CONTENTS

LIST OF TABLES

LIST OF FIGURES

LIST OF SYMBOLS

A	aspect ratio of the cavity, W'/H'
g	gravity acceleration, [m s^{-2}]
H'	height of the cavity, [m]
k	saturated porous medium thermal conductivity, [W m^{-1} K^{-1}]
K	permeability tensor
K_1, K_2	permeability along the principal axes, [m^2]
K^*	permeability ratio, $K^* = K_2/K_1$
Nu	overall Nusselt number, $\int_0^1 (\partial T/\partial x)dy$
Ra	Darcy Rayleigh number, $Ra = gK_2H'\lambda\Delta T'^2/\nu\alpha$
Ra_m	modified Rayleigh number, $Ra_m = 2Ra/(1+K^*)$
T	dimensionless temperature, $(T'-T_l')/\Delta T'$, [K]
T_r', T_l'	temperature at right and left boundaries, [K]
T_m'	temperature of maximum density, [K]
$\Delta T'$	characteristic temperature difference, $T_r'-T_l'$, [K]
t	dimensionless time, $\sigma t'\alpha/H'^2$
u, v	dimensionless velocities components in x and y directions
x, y	dimensionless coordinate system, $x'/H', y'/H'$

Greek symbols:

α	thermal diffusivity $k/(\rho_L C)_f$, [$m^2 s^{-1}$]
ϕ	inclination angle of the cavity
γ	inversion parameter, $\gamma = 2(T'_m - T'_L)/\Delta T'$
λ	thermal expansion coefficient
ν	kinematic viscosity of the fluid, [$m^2 s^{-1}$]
ρ	density of the fluid, [kg m^{-3}]
ψ	stream function

INTRODUCTION

Over the past years considerable research efforts have been devoted to the study of natural convection heat transfer in cavities filled with a fluid-saturated porous medium due to its widespread engineering applications in contemporary technologies. Prominent among these applications are the design of pebble bed nuclear reactors, catalytic reactors, compact heat exchangers, solar power collectors, geothermal energy conversion and research on fibrous materials used in the thermal insulation of buildings. Other examples include geophysical flows, electronic cooling, petroleum reservoir modeling, burying of drums containing heat generating chemicals in the earth, underground spread of pollutants, solidification of casting, power metallurgy, processes of crystal manufacture, foam metals media, storage of agricultural products which generate heat as a result of metabolism, etc.

So far, a substantial part of theoretical and experimental investigations on convective heat transfer in porous media has dealt with the case of isotropic materials [Nield and Bejan, (1992), Bear, (1972), Ingham and Pop, (1999), etc.]. However, in many practical situations the porous materials are anisotropic in their mechanical as well as thermal properties. Anisotropy is generally a consequence of preferential orientation or asymmetric geometry of grain or fibers. For instance, loft insulation has usually a lower permeability across the insulating layer than in the perpendicular directions.

Most of the past studies on natural convection in porous media are concerned with the case of fluids having a linear relationship between density and temperature [Mckibbin and Tyvand, (1982), Nilsen and Storesletten, (1990), Rosenberg and Spera, (1990), Chen et al., (1991), Trew and Mckibbin, (1994), Degan et al., (1995), Bera et al., (1998), etc.]. In general this is a good approximation for most fluids in practical applications. Convection in cold water however behaves in a complicated manner when the temperature domain encompasses the $4°C$ point, at which the density of water reaches a

maximum value. A few other fluids such as gallium, tellurium, antimony and molten bismuth also possess a density extremum in the density-temperature relationship. Convection in such fluids is referred as "inversion density problem".

Inversion density problem

A review on the inversion density problem researches performed during the past years reveals that most of the available studies on this topic focused on the onset of convection in a horizontal layer heated from below (Benard's problem).

As early as 1974, the effects of density inversion on free convective heat transfer in a horizontal porous layer heated below were investigated by Yen, (1974). Glass beads in water composed the saturated porous medium. The effect of density inversion was evaluated by maintaining the upper boundary temperature at $0°C$. The onset of convection was found to depend on two thermal parameters which are functions of the boundary temperatures and the coefficients representing the fluid density –temperature relation. The effect of density inversion on heat transfer rate was found to be significant and to decrease as the temperature difference across the layer increases. For small change of temperature, the effect of density inversion causes heat transfer rate to be as much as 100 percent less than under non-density inversion conditions.

Onset of convection in a horizontal water layer with maximum density effects was performed by Merker et al., (1978). The study is conducted by using a linear stability analysis. The resulting perturbation equations are solved with the aid of Galerkin's method. With the choice of reasonable test functions, it is shown that seven terms are sufficient for an approach close to 1%. The results are represented in terms of stability diagrams. The nonlinear density temperature relation is approximated by three different polynominals having 2, 3, and 5 terms respectively. Assuming the fifth order polynominal to be exact, the critical Rayleigh numbers, calculated with a simple

parabolic relation, are about 10% too large. This discrepancy is reduced to approximately 3% by adding a cubic term to the density-temperature relation.

Finite amplitude natural convection near 4 $^{\circ}C$ in a water saturated porous layer heated from below was investigated by Blake et al., (1984). Their paper reports a numerical study of two-dimensional natural convection in a horizontal porous layer heated from below and saturated with cold water. The top surface is maintained at $0^{\circ}C$ and the bottom one is varied from 4 to 8 $^{\circ}C$. Three separate series of numerical simulations document the effect of Rayleigh number, bottom temperature, and horizontal length of the porous layer on the overall heat transfer rate vertically across the layer.

The effects of inversion density on heat transfer in different kinds of enclosures have been considerably investigated in the past. Results have been obtained for the case of pure water confined in rectangular enclosures [Watson, (1972), Seki et al., (1978), Inaba and Fukuda, (1983), etc.] and in cylindrical annulus [Shekar et al., (1980), Vasseur et al., (1981), etc.]. Also, the case of porous media, which saturated with cold water and confined in a rectangular cavity has been investigated first by Altimir, (1984). Recently, transient natural convection of water near its density extremum, in a rectangular cavity filled with porous medium, was investigated numerically by Chang and Yang, (1995). The top and bottom walls are insulated, and a uniform temperature T_h' is imposed on the left vertical wall while the right wall is maintained at $T_c' = 0\ ^{\circ}C$. The numerical results show that, for $R < 0.5$, the size of the clockwise vortex beside the high-temperature surface increases as time increases. The clockwise vortex occupies almost the whole space when the steady state is reached. For $R = 0.5$, the size of the clockwise vortex adjacent to the high-temperature surface increases as time increases. However, two counter-rotating vortices having the same strength are observed in the cavity when steady state is reached. For $R > 1$, only one counterclockwise vortex exists in the space. Here R

is the maximum density parameter defined as $R=(T'_m-T'_c)/(T'_h-T'_c)$. T'_m, T'_c and T'_h are the maximum density, the cold side and hot side temperature respectively.

Anisotropic porous media

The first study on convective heat transfer within an anisotropic porous media is due to Castinel and Combarnous, (1974), and concentrates on the porous media analogous of the Benard problem. A fluid-saturated porous layer, bounded by two infinite and impermeable horizontal or inclined planes maintained at constant temperatures, was considered. The onset of convection was determined on the basis of linear stability analysis.

Finite amplitude convective heat transfer through an anisotropic porous material in a vertical slot was examined analytically and numerically by Burns et al., (1977). This paper seems to be the first to study the effect of anisotropy on convective flow within a porous medium confined in a two-dimensional rectangular enclosure. The vertical side walls are heated and cooled, respectively, and the horizontal boundaries are insulated or perfectly conducting. The analysis demonstrates the dependence of the Nusselt number on the Rayleigh number, aspect ratio and anisotropic permeabilities. A simple analytical formula for calculating the heat transfer has been developed after obtaining a matching coefficient by comparison with numerical solutions.

Nilsen and Storesletten, (1990), analyzed two-dimensional convection in a horizontal rectangular channel. The channel walls, assumed to be impermeable and perfectly heat conducting, are nonuniformly heated to establish a linear temperature distribution in the vertical direction. It is shown that the critical Rayleigh number and the flow structure at the onset of convection depend on the anisotropy aspect ratio ξ and η defined by

$$\xi = \frac{K_H}{K_V}\left(\frac{h}{a}\right)^2, \qquad \eta = \frac{D_H}{D_V}\left(\frac{h}{a}\right)^2$$

where K_H, K_V, D_H, and D_V are the horizontal and vertical components of the permeability and thermal diffusivity, respectively, and a and h are the horizontal and vertical dimensions of the channel.

A numerical study on natural convection in an enclosure filled with an anisotropic medium was carried out by Ni and Beckermann, (1991). They considered a two-dimensional square cavity where the vertical walls were held isothermally at different temperatures, while the horizontal top and bottom walls were insulated. The effect of mechanical and thermal anisotropy on the streamlines, isotherms and heat transport is studied. The permeability ratio and thermal diffusivity ratio are defined by $K^* = K_V/K_H$, and $k^* = D_V/D_H$, where the subscripts V and H refer to vertical and horizontal directions, respectively. When compared to isotropic porous media, natural convection in the anisotropic case has the following physical characteristics: (1) a high permeability ratio ($K^* > 1$) causes channeling of the flow along the vertical isothermal walls, a higher flow intensity in the enclosure, and consequently a higher Nusselt number. (2) a low permeability ratio ($K^* < 1$) causes channeling of the flow along the horizontal boundaries, thicker velocity boundary layers along the vertical walls, a lower flow intensity in the enclosure and, hence, a smaller Nusselt number. All Nusselt numbers approach unity in the limit $K^* \to 0$. (3) the thermal conductivity and permeability ratios generally have opposing effects on the Nusselt number.

A similar problem was studied numerically by Zhang et al., (1993). They examined convective heat transfer in a two-dimensional rectangular porous cavity, heated from the side. However, it was assumed that the medium is characterized by an anisotropic permeability with inclined axes with respect to the vertical. The streamlines and isotherms at various values of the anisotropy ratio are presented, as well as the

influence of the anisotropy orientation. They also considered Benard convection in a two-dimensional rectangular cavity filled with a porous medium. The horizontal top and bottom walls are cooled and heated respectively, while the vertical walls are insulated. The porous medium is anisotropic in permeability with inclined principal axes. A linear analysis is used to find the marginal stability limit while a finite difference method is applied to numerically simulate the convection flows. When the inclination angle is zero, the critical Rayleigh number is $Ra_c = 2\pi^2(1 + K_T/K_L)$, where, K_L and K_T denote the longitudinal and transverse components of the permeability respectively. Moreover, they found that both the permeability ratio and inclination angle of the principal axes considerably modify the stability limit (Ra_c), the flow pattern and the heat transfer from that under isotropic conditions.

Kimura et al., (1993), made an analysis of natural convection in an anisotropic porous medium by employing a nonlinear perturbation method for small Rayleigh numbers. They consider a two-dimensional porous cavity heated from the side, while the top and bottom walls are insulated. The effects of anisotropy of both permeability and thermal conductivity, and of the geometric aspect ratios on the flow pattern and the heat transfer are documented. In general, it is found that the geometric aspect ratio gives the same effect on the heat transfer and the convective pattern as the anisotropic properties of the porous medium. The results are presented in a number of graphs showing how the streamlines and isotherms depend on the governing parameters, and showing the average Nusselt number variation as a function of Rayleigh number.

Chang and Liu, (1994), made a numerical study to analyze the wall conduction effect of the two-dimensional porous cavity formed by walls having finite conductance. The vertical walls are kept at constant but different temperatures, while the horizontal walls are assumed insulated outside. The numerical results indicate that the anisotropic permeability affects the flow field and heat transfer rate significantly. A critical value of the anisotropic thermal diffusivity ratio D^* may exist such that the Nusselt number

reaches a minimum. The critical value decreases with an increase in the value of the anisotropic permeability ratio K^*. The permeability ratio and thermal diffusivity ratio are defined by $K^* = K_V/K_H$, and $D^* = D_V/D_H$, where the subscripts V and H refer to vertical and horizontal directions, respectively. Moreover, wall conductance effect can lead to large changes in the Nusselt numbers.

Degan et al., (1995), considered the case of a vertical enclosure where the vertical walls are heated and cooled, respectively, by a constant heat flux, while the horizontal walls are insulated. The principal axes of the anisotropic permeability are oblique to the gravity vector, whereas those of the thermal diffusivity coincide with the horizontal and vertical coordinate axes. An analytical solution, valid for flow in slender enclosures, is derived on the basis of a parallel flow approximation while a finite difference method is used to numerically simulate the fluid flow, temperature distribution and heat transfer ratio. A closely related problem has been studied by Degan and Vasseur, (1996). In this case, the vertical walls of the rectangular cavity are heated and cooled isothermally, while the horizontal walls still are insulated. It was shown that both the permeability ratio and inclination angle of the principal axes have a strong influence on the convective flow. Moreover, it is shown that a maximum (minimum) heat transfer within the cavity is obtained when the porous matrix is oriented in such a way that the principal axis with higher permeability is parallel (perpendicular) to the vertical direction. This result is applicable to insulation techniques relative to a vertical porous layer: The best possible insulation is reached when the principal axis with lower permeability is parallel to the vertical direction.

Natural convection in a vertical slot filled with an anisotropic porous medium with oblique principal axes was studied both analytically and numerically, on the basis of the Darcy-Brinkman model by Degan and Vasseur, (1996). The vertical walls of the cavity are heated and cooled isothermally, while the horizontal walls are adiabatic. The porous medium is anisotropic in permeability with its principal axes oriented in a

direction that is oblique to the gravity vector. In the large Rayleigh number limit, a boundary layer solution, based on the integral relations approach developed by Simpkins and Blythe, (1980) is proposed. Scale analysis is applied to predict the order of magnitudes involved in the boundary layer regime. Comparisons between the numerical solutions of the full equations and analytical solutions are presented for a wide range of the governing parameters. The numerical experiments confirm the flow features and scales anticipated properties. It is demonstrated that different orientations of the porous medium considerably modify the flow pattern and heat transfer rate from that expected under isotropic conditions.

The effects of anisotropy on thermal boundary-layer flow in porous media were studied by Ene, (1991). The convective flow is induced by a vertical uniformly heated plate embedded in fluid saturated medium. A combined study of the effects of anisotropic permeability and diffusivity is presented by using the method of integral relations. An analysis is made concerning the validity of the thermal boundary layer approximation in the case of anisotropic medium. It turns out that the boundary layer hypothesis is not valid if the permeability along the plate, K_x, is much greater than the permeability in the direction orthogonal to the plate, K_y. It is shown that if $K_y > K_x$, there is an increase in the temperature field compared to the case of $K_y < K_x$.

Also, some papers have analyzed the influences of hydrodynamic dispersion on convection in anisotropic media, [Fattah and Hoopes, (1985) and Howle and Georgiadis,(1994)]. Double-diffusive convection in an anisotropic porous medium was studied by Trevisan and Bejan, (1985), Nguyen et al., (1991), Costa, (1997), Fard et al., (1997), and Bera et al., (1998), etc.. The researches on convective flow through anisotropic porous media has been reviewed recently by Storesletten,(1999).

Outline of thesis

Relatively little work has been done to study the effects of the density inversion on the thermal convection within anisotropic porous medium in spite of their common occurrence in northern climates like those prevailing in Canada. Unusual flow patterns may be expected in areas of water exposed to near freezing temperatures. An understanding of mechanisms of such flow is of practical interest due to the problems arising in cryogenic heat exchanger operations, the freezing of rivers and lakes, the design of utility systems, etc.

The problem of thermal convection within an anisotropic porous medium filled with water near its maximum density is considered in this study. The Darcy's flow model and a parabolic density temperature relation will be used here. The present study will be done numerically.

Chapter 1 presents the mathematical model for natural convection of cold water within an anisotropic porous medium confined in an inclined rectangular cavity. Both dimensional and dimensionless forms of the governing equations are presented. The definition of the inversion parameter γ is introduced in this chapter. Chapter 2 contains the numerical scheme used to solve the governing equations given in Chapter 1. A test study is done here in order to verify the current numerical approach. In Chapter 3, a particular case of a vertical cavity is considered and the conclusions and recommendations are outlined in Chapter 4.

CHAPTER I

MATHEMATICAL MODEL

The physical system of interest is shown in Figure 1.1. It consists in a rectangular cavity filled with a water-saturated porous medium, anisotropic in permeability. The cavity is of height H', width W', and tilted at an angle ϕ with respect to the horizontal plane. The permeabilities along the two principal axes of the porous matrix are denoted by K_1 and K_2, and the anisotropy ratio is then defined as $K^* = K_2 / K_1$. The orientation angle θ is defined in Figure 1.1. The top and bottom boundaries are adiabatic, and the other boundaries are maintained at constant uniform temperatures T_l' and T_r' respectively.

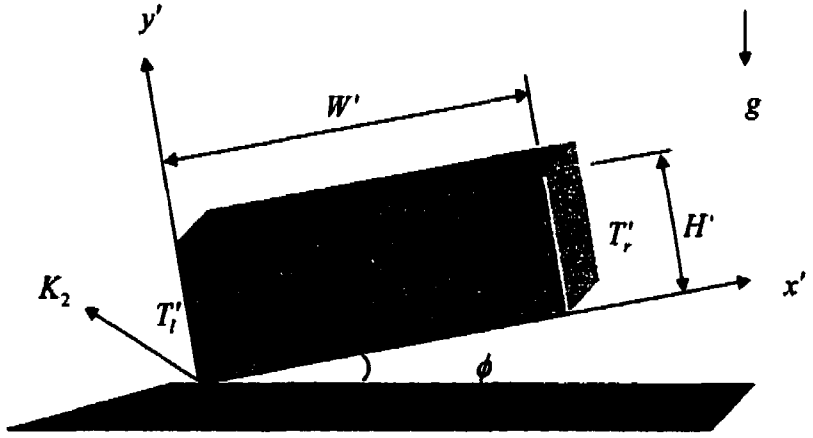

Figure 1.1 The definition of the problem

The motion of water through the porous medium obeys Darcy's law. The porous medium is saturated with water in local thermodynamic equilibrium with the solid matrix. The assumption of a Boussinesq incompressible fluid is adopted for water and physical properties other than the density in the buoyancy force are supposed constant. The density is considered to vary with the temperature according to a parabolic relationship of the form:

$$\frac{\rho-\rho_m}{\rho_m}=\lambda(T'-T'_m)^2 \tag{1.1}$$

where ρ_m is the maximum density corresponding to the temperature $T'_m=3.98^oC$, and $\lambda=7.94\times10^{-6}(^oC)^2$ for water. The resulting equation is considered valid for the range $0-8^oC$ (Moore and Weiss, 1973).

The continuity, momentum and energy equations that govern the flow and heat transfer inside the enclosure are:

$$\nabla\cdot\vec{V}'=0 \tag{1.2}$$

$$\vec{V}'=\frac{\overline{\overline{K'}}}{\mu}(-\nabla P'+\rho\vec{g}) \tag{1.3}$$

$$(\rho c)_p\frac{\partial T'}{\partial t'}+(\rho c)_f\nabla\cdot(\vec{V}'T')=k\nabla^2T' \tag{1.4}$$

In the above equations, $\vec{V}'$ is the mass averaged velocity, $\vec{g}$ the gravity vector, $(\rho c)_f$ the thermal capacity of the saturating fluid with the reference density, $(\rho c)_p$ the thermal capacity of the saturated porous medium, k the thermal conductivity of the saturated porous medium, and $\overline{\overline{K'}}$ the second order permeability tensor defined as:

$$\overline{\overline{K'}}=\begin{bmatrix} K_1\cos^2\theta+K_2\sin^2\theta & (K_1-K_2)\sin\theta\cos\theta \\ (K_1-K_2)\sin\theta\cos\theta & K_1\sin^2\theta+K_2\cos^2\theta \end{bmatrix} \tag{1.5}$$

The unknown variables of the present problem are the velocity components (u',v'), pressure P' and temperature T'.

1.1 Momentum equation

The pressure term appearing in the momentum Eq.(1.3) can be expressed as:

$$P' = P'_0 - \rho_0 g z' + P'_r \tag{1.6}$$

with the following definitions:

P'_0 reference pressure

ρ_0 reference density $\rho_0 = \rho + \Delta\rho$

P'_r residual pressure

z' coordinate in vertical direction

From the above equation, it follows that

$$\nabla P' = \nabla P'_r - \nabla \rho_0 g z' \tag{1.7}$$

and the gravity term in the momentum equation (1.3) becomes:

$$\rho \vec{g} = (\rho_0 - \Delta\rho)\vec{g} \tag{1.8}$$

Substituting Eqs (1.7) and (1.8) in to the momentum equation (1.3) yields

$$\vec{V}' = -\frac{\overline{\overline{K'}}}{\mu}(\nabla P' + \Delta\rho g \hat{z}) \tag{1.9}$$

where P' is the residual pressure, its subscript r being dropped, and $\hat{z}$ is the unit vector in the vertical direction.

The permeability tensor may be expressed as $\overline{\overline{K'}} = K_2 \overline{\overline{K}}$, in which

$$\overline{\overline{K}} = \begin{bmatrix} \frac{1}{K^*}\cos^2\theta + \sin^2\theta & (\frac{1}{K^*} - 1)\sin\theta\cos\theta \\ (\frac{1}{K^*} - 1)\sin\theta\cos\theta & \frac{1}{K^*}\sin^2\theta + \cos^2\theta \end{bmatrix} \tag{1.10}$$

is a dimensionless form of the permeability tensor.

The inverse of $\overline{\overline{K}}$ is defined as:

$$\overline{\overline{R}} = \begin{bmatrix} K^*\cos^2\theta + \sin^2\theta & (K^* - 1)\sin\theta\cos\theta \\ (K^* - 1)\sin\theta\cos\theta & K^*\sin^2\theta + \cos^2\theta \end{bmatrix} = \left(\overline{\overline{K}}\right)^{-1} \tag{1.11}$$

is called the hydraulic resistivity tensor (Bear, 1972). This tensor may be considered as the sum of two tensors:

$$\overline{\overline{R}} = \begin{bmatrix} 1 & 0 \\ 0 & 1 \end{bmatrix} + \left(K^* - 1\right)\begin{bmatrix} \cos^2\theta & \sin\theta\cos\theta \\ \sin\theta\cos\theta & \sin^2\theta \end{bmatrix} \tag{1.12}$$

The first term is the identity matrix, which stands for an isotropic medium with permeability K_2. The second term is the true anisotropic contribution. With $K_1 < K_2$, this second term is positive as it should, an added hydraulic resistivity to the flow being brought to the system.

With the definition (1.11), Eq. (1.9) becomes:

$$\begin{bmatrix} K^{*}\cos^2\theta+\sin^2\theta & (K^{*}-1)\sin\theta\cos\theta \\ (K^{*}-1)\sin\theta\cos\theta & K^{*}\sin^2\theta+\cos^2\theta \end{bmatrix} \begin{Bmatrix} u' \\ v' \end{Bmatrix} = -\frac{K_2}{\mu} \begin{Bmatrix} \frac{\partial P'}{\partial x'}+\Delta\rho g\sin\phi \\ \frac{\partial P'}{\partial y'}+\Delta\rho g\cos\phi \end{Bmatrix} \quad (1.13)$$

Momentum Eq.(1.9) takes the following forms in the x and y directions:

x direction:

$$(K^{*}\cos^2\theta+\sin^2\theta)u'+((K^{*}-1)\sin\theta\cos\theta)v' = -\frac{K_2}{\mu}\left[\frac{\partial p'}{\partial x'}+\Delta\rho g\sin\phi\right] \quad (1.14)$$

y direction:

$$((K^{*}-1)\sin\theta\cos\theta)u'+(\cos^2\theta+K^{*}\sin^2\theta)v' = -\frac{K_2}{\mu}\left[\frac{\partial p'}{\partial y'}+\Delta\rho g\cos\phi\right] \quad (1.15)$$

By defining the following coefficients

$$\begin{aligned} a &= \cos^2\theta+K^{*}\sin^2\theta \\ b &= (1-K^{*})\sin 2\theta \\ c &= K^{*}\cos^2\theta+\sin^2\theta \end{aligned} \quad (1.16)$$

Eq. (1.12), (1.13) and (1.14) take the condensed forms:

$$\begin{bmatrix} c & -\frac{b}{2} \\ -\frac{b}{2} & a \end{bmatrix} \begin{bmatrix} u' \\ v' \end{bmatrix} = -\frac{K_2}{\mu} \begin{bmatrix} \frac{\partial P'}{\partial x'}+\Delta\rho g\sin\theta \\ \frac{\partial P'}{\partial y'}+\Delta\rho g\cos\theta \end{bmatrix} \quad (1.12a)$$

$$cu' - \frac{b}{2}v' = -\frac{K_2}{\mu}\left[\frac{\partial p'}{\partial x'} + \Delta\rho g \sin\phi\right] \tag{1.13a}$$

$$-\frac{b}{2}u' + av' = -\frac{K_2}{\mu}\left[\frac{\partial p'}{\partial y'} + \Delta\rho g \cos\phi\right] \tag{1.14a}$$

Taking the curl of the Eq. (1.12a) and eliminating the pressure term we get:

$$-a\frac{\partial v'}{\partial x'} + \frac{b}{2}\left(\frac{\partial u'}{\partial x'} - \frac{\partial v'}{\partial y'}\right) + c\frac{\partial u'}{\partial y'} = \frac{K_2 g}{\nu}\left[\cos\phi\frac{\partial}{\partial x'} - \sin\phi\frac{\partial}{\partial y'}\right]\frac{\Delta\rho}{\rho_0} \tag{1.17}$$

In the present study, the density is considered to vary with the temperature according to the non-linear parabolic relationship given by Eq. (1.1). Using an arbitrary reference density ρ_0, we can write

$$\frac{\rho_m - \rho}{\rho_0} \approx \frac{\rho_m - \rho_0}{\rho_m} = \lambda(T' - T_m')^2 \tag{1.18}$$

and consequently:

$$\frac{\rho - \rho_m}{\rho_0} = \frac{\rho - \rho_0}{\rho_0} + \frac{\rho_0 - \rho_m}{\rho_0} = -\lambda(T' - T_m')^2 \tag{1.19}$$

We can express the temperature difference in Eq. (1.19) as follows:

$$(T' - T_m')^2 = \left[(T' - T_0') + (T_0' - T_m')\right]^2 = (T' - T_0')^2 + 2(T_0' - T_m')(T' - T_0') + (T_0' - T_m')^2$$

so that Eq. (1.19) becomes:

$$\frac{\rho-\rho_0}{\rho_0}+\frac{\rho_0-\rho_m}{\rho_0}=-\lambda(T'-T_0')^2-2\lambda(T_0'-T_m')(T'-T_0')-\lambda(T_0'-T_m')^2$$

This last expression may be simplified by the use of Eq. (1.18) to give:

$$\frac{\rho-\rho_0}{\rho_0}=-\lambda(T'-T_0')^2-2\lambda(T_0'-T_m')(T'-T_0') \tag{1.20}$$

Let $T_0'=T_r'$, $\rho_0=\rho_r$ and $\Delta T'=T_l'-T_r'$; then we define the following dimensionless temperature:

$$T=\frac{T'-T_r'}{\Delta T'} \tag{1.21}$$

Eq. (1.20) may then be written as:

$$\frac{\rho-\rho_r}{\rho_r}=-\lambda\Delta T'^2\left[-2\left(\frac{T_m'-T_r'}{\Delta T'}\right)T+T^2\right] \tag{1.22}$$

By introducing the inversion parameter defined as:

$$\gamma=2\frac{T_m'-T_r'}{\Delta T'} \tag{1.23}$$

Eq. (1.22) becomes:

$$\frac{\Delta\rho}{\rho_0}=\frac{\rho-\rho_r}{\rho_r}=-\lambda\Delta T'^2(T^2-\gamma T) \tag{1.24}$$

We can express the velocity terms u', v' in terms of the stream function:

$$u' = \frac{\partial \psi'}{\partial y'} \text{ and } v' = -\frac{\partial \psi'}{\partial x'} \tag{1.25}$$

such a definition automatically satisfies the continuity equation. Replacing $\Delta\rho/\rho_0$ and u', v' by their respectively expressions Eq. (1.24) and (1.25) in Eq. (1.17) yields:

$$a\frac{\partial^2 \psi'}{\partial x'^2} + b\frac{\partial^2 \psi'}{\partial x' \partial y'} + c\frac{\partial^2 \psi'}{\partial y'^2} = \frac{g\lambda H' K_2 \Delta T'^2}{\alpha \nu}(\gamma - 2T)\left[\cos\phi \frac{\partial T}{\partial x'} - \sin\phi \frac{\partial T}{\partial y'}\right] \tag{1.26}$$

1.2 Energy equation

By introducing the thermal capacity $\sigma = (\rho c)_p/(\rho c)_f$ and the thermal diffusivity $\alpha = k/(\rho c)_f$ the energy equation becomes:

$$\sigma\frac{\partial T'}{\partial t'} + \nabla \cdot (\vec{V}'T') = \alpha \nabla^2 T' \tag{1.27}$$

The Nusselt number is defined as:

$$Nu = \frac{Q'_{conv}}{Q'_{cond}} \tag{1.28}$$

The local value takes the following form:

$$Nu_{local} = (-k\frac{\partial T'}{\partial x'})\Big/(-k\frac{T'_i - T'_r}{W'}) \tag{1.29}$$

and the overall Nusselt number becomes:

$$Nu = \int_0^{H'} Nu_{local} dy' \tag{1.30}$$

1.3 Dimensionless equations

Finally, the equations mentioned above are put in dimensionless form by defining the following set of new variables:

$$\begin{aligned}
&(x, y) = (x', y')/H' \\
&\psi = \psi'/\alpha \\
&T = (T' - T_r')/\Delta T' \\
&t = t'/(\frac{H'^2\sigma}{\alpha}) \\
&(u, v) = \frac{H'}{\alpha}(u', v')
\end{aligned} \tag{1.31}$$

The dimensional variables represented by prime quantities in previous governing Eqs. (1.26) and (1.27)are replaced by new dimensionless (unprimed) variables in Eq. (1.31), and the following dimensionless governing equations are obtained:

Momentum equation:

$$a\frac{\partial^2\psi}{\partial x^2} + b\frac{\partial^2\psi}{\partial x\partial y} + c\frac{\partial^2\psi}{\partial y^2} = Ra(\gamma - 2T)\left[\cos\phi\frac{\partial T}{\partial x} - \sin\phi\frac{\partial T}{\partial y}\right] \tag{1.32}$$

Energy equation:

$$\frac{\partial T}{\partial t}+\nabla\cdot(\vec{V}T)=\nabla^2 T \tag{1.33}$$

In Eq. (1.32), $Ra = gK_2H'\lambda\Delta T'^2/\alpha\nu$ is the Darcy's Rayleigh number.

The heat transfer rate between the left and right walls is given by the overall Nusselt number, defined as:

$$Nu=\int_0^1 \frac{\partial T}{\partial x}dy \tag{1.34}$$

Governing parameters of the present problem are the Rayleigh number Ra, the inversion parameter γ, the permeability ratio K^*, the orientation angle of the principal axes θ, and the inclination angle ϕ.

1.4 Boundary conditions

Hydrodynamic boundary conditions on all solid boundaries are

$$\psi=\frac{\partial \psi}{\partial n}=0 \tag{1.35}$$

where n is the direction normal to the boundary

The thermal boundary conditions are given by

$$\begin{aligned} &x=0,\ A: && T=1,0\\ &y=0,\ 1: && \frac{\partial T}{\partial y}=0 \end{aligned} \tag{1.36}$$

1.5 Limiting cases

If the inversion density parameter γ increases to large values, then the temperature term in Eq. (1.32) will be comparatively small, and the problem reaches the asymptotic classical behavior of a density linearly related to temperature. The momentum equation becomes:

$$a\frac{\partial^2\psi}{\partial x^2}+b\frac{\partial^2\psi}{\partial x\partial y}+c\frac{\partial^2\psi}{\partial y^2}=Ra\gamma\left[\cos\phi\frac{\partial T}{\partial x}-\sin\phi\frac{\partial T}{\partial y}\right] \tag{1.37}$$

The standard case of linear convection is thus recovered with $Ra_l = \lim_{\gamma\to\pm\infty}\left|\ \gamma\ Ra\ \right|$, Ra_l being the standard form of the Darcy Rayleigh number:

$$Ra_l=\frac{gK_2H'\beta\Delta T'}{\alpha\nu} \tag{1.38}$$

Setting the permeability ratio $K^* = 1$, reduces the momentum equation Eq.(1.32) to the standard form valid for an isotropic porous medium. The momentum equation becomes:

$$\frac{\partial^2\psi}{\partial x^2}+\frac{\partial^2\psi}{\partial y^2}=Ra(\gamma-2T)\left[\cos\phi\frac{\partial T}{\partial x}-\sin\phi\frac{\partial T}{\partial y}\right] \tag{1.39}$$

CHAPTER II

NUMERICAL APPROACH

The general equations governing the conservation of mass, momentum and energy in the present problem have been discussed in the previous chapter. An important task we are facing now is to devise numerical techniques for solving these equations subjected to appropriate boundary conditions. As stated in the previous chapter, the treatment will be limited to the case of two-dimensional incompressible flows.

Aside from numerical techniques, experimental investigations or analytical approaches can also predict heat transfer and fluid flow processes. Analytical solutions are sometimes possible when the complexity of the governing equations is reduced through simplifying assumptions. Such assumptions are necessary to make the problem tractable, but they severely limit the applicability of the approach.

Experimental investigation can provide information regarding a particular problem of interest. However, the limitation on hardware required for the model and the complexity in simulating adequately the prototype, make it a difficult task to obtain reliable results. Nevertheless, the information obtained from the experiments is extremely valuable in validating the numerical and analytical solutions of the governing equations.

The availability of the computer has stimulated the rapid growth of the numerical or computational approaches to solve complex problems in heat transfer. With the development of computer science, the introduction of improved numerical techniques is being proposed almost on daily basis.

There are various numerical techniques to discretize and solve the equations governing the present problem, among which the finite difference approach is the most

straightforward method. This chapter will provide an overview of the role and nature of the numerical techniques in terms of finite difference approach. A detailed description of a numerical procedure, that can handle the specific problem considered in this work as well as a wide variety of engineering problems is then presented.

2.1 Finite difference methods

In the finite difference approach, the flow domain is discretized so that the dependent variables are considered only at discrete points. The typical two-dimensional grid system is shown in Figure 2.1, where (i, j) is the grid point in rectangular coordinates and the superscript n indicates the time-marching coordinate. Derivatives are approximated by differences resulting in an algebraic representation of the partial differential equation (PDE).

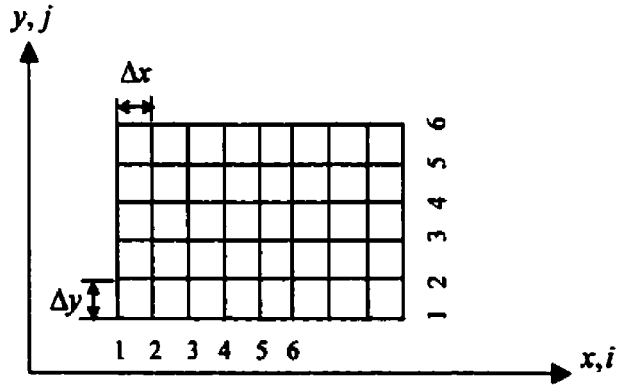

Figure 2.1 Arrangement of the grid points

The second-order central difference approximation is a frequently used scheme for solving the governing equations described in Chapter 1. However, in the convection dominated flow (High Peclet, Reynolds, or Rayleigh numbers), using the second-order central difference approximation to discretize the convection terms in the governing equations may produce wiggle solutions.

2.1.1 Discretization of governing equations

For numerical computation, the governing differential equations have to be cast in a discrete form. Owing to the moderate convection flow of the present problem, all the convection and diffusive terms in the equations are discretized by Taylor-series, second order central difference scheme, while the time derivatives are approximated by forward differences.

A. Momentum equation

For the momentum Eq. (1.32)

$$a\frac{\partial^2\psi}{\partial x^2}+b\frac{\partial^2\psi}{\partial x\partial y}+c\frac{\partial^2\psi}{\partial y^2}=Ra(\gamma-2T)\left[\cos\phi\frac{\partial T}{\partial x}-\sin\phi\frac{\partial T}{\partial y}\right]$$

the following central finite difference formulas are used:

$$(f_x)_{i,j}=\frac{\partial f}{\partial x}=\frac{f_{i+1,j}-f_{i-1,j}}{2\Delta x}+o(\Delta x^2)$$

$$(f_{xx})_{i,j}=\frac{\partial^2 f}{\partial x^2}=\frac{f_{i-1,j}-2f_{i,j}+f_{i+1,j}}{\Delta x^2}+o(\Delta x^2)$$

$$(f_{xy})_{i,j}=\frac{f_{i+1,j+1}-f_{i+1,j-1}-f_{i-1,j+1}+f_{i-1,j-1}}{4\Delta x\Delta y} \qquad (2.1)$$

$$(\frac{\partial T}{\partial x})_{i,j} = \frac{(T_{i+1,j}^{n+1} - T_{i-1,j}^{n+1})}{2\Delta x}$$

$$(\frac{\partial T}{\partial y})_{i,j} = \frac{(T_{i,j+1}^{n+1} - T_{i,j-1}^{n+1})}{2\Delta y}$$

As a result, the left side of stream function becomes:

$$a\frac{\psi_{i-1,j} - 2\psi_{i,j} + \psi_{i+1,j}}{\Delta x^2} + b\frac{\psi_{i+1,j+1} - \psi_{i+1,j-1} - \psi_{i-1,j+1} + \psi_{i-1,j-1}}{4\Delta x\Delta y} + c\frac{\psi_{i,j-1} - 2\psi_{i,j} + \psi_{i,j+1}}{\Delta y^2}$$

while the right side of equation is given by:

$$Ra(\gamma - 2T)\left[\left(\frac{T_{i+1,j} - T_{i-1,j}}{2\Delta x}\right)\cos\phi - \left(\frac{T_{i,j+1} - T_{i,j-1}}{2\Delta y}\right)\sin\phi\right]$$

Thus it is easily found that:

$$\psi_{i,j} = A(\psi_{i-1,j} + \psi_{i+1,j}) + B(\psi_{i+1,j+1} - \psi_{i+1,j-1} - \psi_{i-1,j+1} + \psi_{i-1,j-1}) + C(\psi_{i,j-1} + \psi_{i,j+1}) +$$
$$D\left[\left(\frac{T_{i+1,j} - T_{i-1,j}}{2\Delta x}\right)\cos\phi - \left(\frac{T_{i,j+1} - T_{i,j-1}}{2\Delta y}\right)\sin\phi\right] \qquad (2.2)$$

where
$$A = a\frac{\Delta y^2}{2(a\Delta y^2 + c\Delta x^2)}$$

$$B = b\frac{\Delta x\Delta y}{8(a\Delta y^2 + c\Delta x^2)}$$

$$C = c\frac{\Delta x^2}{2(a\Delta y^2 + c\Delta x^2)} \qquad (2.3)$$

$$D = Ra(\gamma - 2T)\frac{\Delta x^2 \Delta y^2}{2(a\Delta y^2 + c\Delta x^2)}$$

In order to accelerate the convergence to the solution of the above equation, we introduce the successive over-relaxation method (SOR) (Carnahan, et al., 1969). The value of stream function at point (i, j) for the time step $(k+1)\Delta t$ is then given by:

$$\psi_{i,j}^{k+1} = (1-\omega)\psi_{i,j}^{k} + \omega\psi_{i,j} \tag{2.4}$$

where, ω is the over-relaxation coefficient given by:

$$\omega = \frac{2}{\xi^2}(1-\sqrt{1-\xi^2}) \tag{2.5}$$

where

$$\xi = \frac{2\cos(\pi/n_x) + \Delta x^2/\Delta y^2 \cos(\pi/n_y)}{1+\Delta x^2/\Delta y^2} \tag{2.6}$$

In the above equation, n_x and n_y are the numbers of grid points in x and y directions, respectively.

B. Energy equation

The energy equation is given by Eq.(1.33)

$$\frac{\partial T}{\partial t} + \nabla\cdot(\vec{V}T) = \nabla^2 T$$

Using the discrete form mentioned above, the terms in the energy equation can be discretized as:

$$
\begin{aligned}
(\frac{\partial T}{\partial t})_{i,j} &= \frac{T_{i,j}^{n+1} - T_{i,j}^{n}}{\Delta t} \\
(\frac{\partial uT}{\partial x})_{i,j} &= \frac{u_{i+1,j}^{n} T_{i+1,j}^{n+1} - u_{i-1,j}^{n} T_{i-1,j}^{n+1}}{2\Delta x} \\
(\frac{\partial vT}{\partial y})_{i,j} &= \frac{v_{i,j+1}^{n} T_{i,j+1}^{n+1} - v_{i,j-1}^{n} T_{i,j-1}^{n+1}}{2\Delta y} \\
(\nabla^2 T)_{i,j} &= \frac{T_{i+1,j}^{n+1} - 2T_{i,j}^{n+1} + T_{i-1,j}^{n+1}}{\Delta x^2} + \frac{T_{i,j+1}^{n+1} - 2T_{i,j}^{n+1} + T_{i,j-1}^{n+1}}{\Delta y^2}
\end{aligned}
\tag{2.7}
$$

Substituting Eq (2.7) into the energy equation, it is found that:

$$
\begin{aligned}
&\frac{T_{i+1,j}^{n+1} - 2T_{i,j}^{n+1} + T_{i-1,j}^{n+1}}{\Delta x^2} + \frac{T_{i,j+1}^{n+1} - 2T_{i,j}^{n+1} + T_{i,j-1}^{n+1}}{\Delta y^2} = \frac{T_{i,j}^{n+1} - T_{i,j}^{n}}{\Delta t} + \frac{u_{i+1,j}^{n} T_{i+1,j}^{n+1} - u_{i-1,j}^{n} T_{i-1,j}^{n+1}}{2\Delta x} \\
&+ \frac{v_{i,j+1}^{n} T_{i,j+1}^{n+1} - v_{i,j-1}^{n} T_{i,j-1}^{n+1}}{2\Delta y}
\end{aligned}
\tag{2.8}
$$

From the above equation, it follows that:

$$
a_{i,j} T_{i+1,j}^{n+1} + b_{i,j} T_{i-1,j}^{n+1} + c_{i,j} T_{i,j}^{n+1} + d_{i,j} T_{i,j-1}^{n+1} + e_{i,j} T_{i,j+1}^{n+1} = f_{i,j} \tag{2.9}
$$

where the coefficients in the above equation are given by:

$$
a_{i,j} = \frac{u_{i+1,j}^{n}}{2\Delta x} - \frac{1}{\Delta x^2}
$$

$$b_{i,j} = -\frac{u^n_{i-1,j}}{2\Delta x} - \frac{1}{\Delta x^2}$$

$$c_{i,j} = \frac{1}{\Delta t} + \frac{2}{\Delta x^2} \qquad (2.10)$$

$$d_{i,j} = -\frac{v^n_{i,j-1}}{2\Delta y} - \frac{1}{\Delta y^2}$$

$$f_{i,j} = \frac{T^n_{i,j}}{\Delta t}$$

It is obvious that the coefficient matrix in the above equations is pentadiagonal. The solution procedure to solve these equations is time-consuming. One way to overcome the shortcoming and inefficiency of the method mentioned above, is to use a splitting method. This method is known as the Alternating Direction Implicit method (ADI) (Patankar, 1980). The algorithm produces two sets of tridiagonal simultaneous equations to be solved in sequence. The finite difference form of the energy equation in the ADI formulation, with the second order truncation $\Delta t^2, \Delta x^2$, and Δy^2, is given by:

Implicit in x direction at the first half time step:

$$\frac{T^{n+\frac{1}{2}}_{i+1,j} - 2T^{n+\frac{1}{2}}_{i,j} + T^{n+\frac{1}{2}}_{i-1,j}}{\Delta x^2} + \frac{T^n_{i,j+1} - 2T^n_{i,j} + T^n_{i,j-1}}{\Delta y^2} = \frac{T^{n+\frac{1}{2}}_{i,j} - T^n_{i,j}}{\Delta t/2} + \frac{u^n_{i+1,j}T^{n+\frac{1}{2}}_{i+1,j} - u^n_{i-1,j}T^{n+\frac{1}{2}}_{i-1,j}}{2\Delta x}$$

$$+ \frac{v^n_{i,j+1}T^n_{i,j+1} - v^n_{i,j-1}T^n_{i,j-1}}{2\Delta y} \qquad (2.11)$$

Implicit in y direction at the last half time step:

$$\frac{T_{i+1,j}^{n+\frac{1}{2}} - 2T_{i,j}^{n+\frac{1}{2}} + T_{i-1,j}^{n+\frac{1}{2}}}{\Delta x^2} + \frac{T_{i,j+1}^{n+1} - 2T_{i,j}^{n+1} + T_{i,j-1}^{n+1}}{\Delta y^2} = \frac{T_{i,j}^{n+1} - T_{i,j}^{n+\frac{1}{2}}}{\Delta t/2}$$

$$+ \frac{u_{i+1,j}^{n} T_{i+1,j}^{n+\frac{1}{2}} - u_{i-1,j}^{n} T_{i-1,j}^{n+\frac{1}{2}}}{2\Delta x} + \frac{v_{i,j+1}^{n} T_{i,j+1}^{n+1} - v_{i,j-1}^{n} T_{i,j-1}^{n+1}}{2\Delta y} \qquad (2.12)$$

We can write these equations in tri-diagonal forms:

$$A_1 T_{i-1,j}^{n+\frac{1}{2}} + B_1 T_{i,j}^{n+\frac{1}{2}} + C_1 T_{i+1,j}^{n+\frac{1}{2}} = D_1 \qquad (2.13)$$

where $A_1 = \frac{1}{\Delta x^2} + \frac{u_{i-1,j}^{n}}{2\Delta x}$

$$B_1 = -\frac{2}{\Delta x^2} - \frac{2}{\Delta t} \qquad (2.14)$$

$$C_1 = \frac{1}{\Delta x^2} + \frac{u_{i+1,j}^{n}}{2\Delta x}$$

$$D_1 = \left(\frac{-1}{\Delta y^2} + \frac{-v_{i,j-1}^{n}}{2\Delta y}\right) T_{i,j-1}^{n} + \left(\frac{2}{\Delta y^2} - \frac{2}{\Delta t}\right) T_{i,j}^{n} + \left(\frac{-1}{\Delta y^2} + \frac{v_{i,j+1}^{n}}{2\Delta y}\right) T_{i,j+1}^{n}$$

and

$$A_2 T_{i,j-1}^{n+1} + B_2 T_{i,j}^{n+1} + C_2 T_{i,j+1}^{n+1} = D_2 \qquad (2.15)$$

where

$$A_2 = \frac{1}{\Delta y^2} + \frac{v_{i,j-1}^{n}}{2\Delta y}$$

$$B_2 = \frac{-2}{\Delta y^2} + \frac{-2}{\Delta t} \qquad (2.16)$$

$$C_2 = \frac{1}{\Delta y^2} + \frac{v^n_{i,j+1}}{2\Delta y}$$

$$D_2 = (\frac{-1}{\Delta x^2} + \frac{-u^n_{i-1,j}}{2\Delta x})T^{n+\frac{1}{2}}_{i-1,j} + (\frac{2}{\Delta x^2} - \frac{2}{\Delta t})T^{n+\frac{1}{2}}_{i,j} + (\frac{-1}{\Delta x^2} + \frac{u^n_{i+1,j}}{2\Delta x})T^{n+\frac{1}{2}}_{i,j+1}$$

2.2 Nusselt number

For the local Nusselt number anywhere along the vertical boundary $Nu = \partial T/\partial x$, we can use the second order or the third order derivative form. See the Fig. 2.1. The second order for the x direction for example is given by:

$$f'_x = \frac{T_3 - 4T_2 + 3T_1}{2\Delta x} \tag{2.17}$$

while the third order is :

$$f'_x = \frac{2T_4 - 9T_3 + 18T_2 - 11T_1}{6\Delta x} \tag{2.18}$$

At last the overall Nusselt number on a given boundary is calculated by the following Simpson integration method,

$$\int_a^b f(x)dy = \frac{\Delta y}{3}[f(a) + 4f(a+\Delta y) + f(b)] \tag{2.19}$$

the Simpson integrating method yields:

$$\int_{y_1}^{y_n} f(x)dy = \sum_{i=1,3,5}^{n-2} \frac{y_{i+1} - y_i}{3}[f(y_i) + 4f(y_{i+1}) + f(y_{i+2})] \tag{2.20}$$

Thus the overall Nuselt number is given as:

$$Nu = \int_0^1 f(x)dy = \frac{\Delta y}{3}[f(y_{NY+1}) + f(y_1) + 4f(y_{even}) + 2f(y_{odd})\ ] \tag{2.21}$$

2.3 Boundary conditions

A. Temperature

The discretization form of the temperature at boundary points, for instance, in x direction (see the Figure 2.1) is calculated from the following equations

$$T_2 = T_1 + (\frac{\partial T}{\partial x})_1 \Delta x + \frac{1}{2}(\frac{\partial^2 T}{\partial x^2})_1 \Delta x^2 + o(\Delta x^3) \tag{2.22}$$

$$T_3 = T_1 + (\frac{\partial T}{\partial x})_1 (2\Delta x)\Delta x + \frac{1}{2}(\frac{\partial^2 T}{\partial x^2})_1 (2\Delta x)^2 + o((2\Delta x)^3) \tag{2.23}$$

Subtracting T_3 from $4T_2$, then we get the equation for the temperature at the boundary point.

$$T_1 = \frac{1}{3}(4T_2 - T_3 - 2\Delta x(\frac{\partial T}{\partial x})_1) \tag{2.24}$$

As discussed in Chapter 1, the enclosure boundaries, which are parallel to the x axis, are adiabatic. This means that $\partial T/\partial y = 0$, at $y = 0,\ 1$. So, at $j = 1$, and $j = Ny+1$, we have:

$$T_{i,1} = \frac{1}{3}(4T_{i,2} - T_{i,3}) \tag{2.25}$$

and

$$T_{i,Ny+1} = \frac{1}{3}(4T_{i,Ny} - T_{i,Ny-1}) \tag{2.26}$$

Other boundaries, which are perpendicular to the x axis, are maintained at constant uniform temperature $T_l = 1$ and $T_r = 0$ respectively. Thus we have $T_{1,j} = T_l = 1$ at $x = 0$ and $T_{Nx+1,j} = T_r = 0$ at $x = A$.

B. Velocity

The velocity is calculated from the stream function using the relations $u = \partial\psi/\partial y$ and $v = -\partial\psi/\partial x$. It is found that:

$$u_{i,j}^{n+1} = \frac{\psi_{i,j+1}^{n+1} - \psi_{i,j-1}^{n+1}}{2\Delta y} \tag{2.27}$$

$$v_{i,j}^{n+1} = \frac{\psi_{i+1,j}^{n+1} - \partial\psi_{i-1,j}^{n+1}}{2\Delta x} \tag{2.28}$$

For the velocities on boundaries, using the similar method, which deals with temperature located at boundary. Near the boundaries which are perpendicular to the x axis, for instance, the stream functions have the following relationships: (See Figure 2.1)

$$\psi_{2,j} = \psi_{1,j} + \left(\frac{\partial \psi}{\partial x}\right)_{1,j} \Delta x + \frac{1}{2}\left(\frac{\partial \psi}{\partial x}\right)^2_{1,j} \Delta x^2 \tag{2.29}$$

$$\psi_{3,j} = \psi_{1,j} + \left(\frac{\partial \psi}{\partial x}\right)_{1,j} 2\Delta x + \frac{1}{2}\left(\frac{\partial \psi}{\partial x}\right)^2_{1,j} (2\Delta x)^2 \tag{2.30}$$

From these two equations, the velocities at the boundary can be calculated by:

$$v_{1,j} = -\left(\frac{\partial \psi}{\partial x}\right)_{1,j} = \frac{\psi_{3,j} - 4\psi_{2,j} + 3\psi_{1,j}}{2\Delta x} \tag{2.31}$$

In the same way, we can calculate all velocities at other boundaries $x = 1$, $y = 0$, and $y = 1$ respectively:

$$v_{N_x+1,j} = \frac{4\psi_{N_x,j} - \psi_{N_x-1,j} - 3\psi_{N_x+1,j}}{2\Delta x} \tag{2.32}$$

$$u_{i,1} = \frac{\psi_{i,3} - 4\psi_{i,2} + 3\psi_{i,1}}{2\Delta x} \tag{2.33}$$

$$u_{i,N_y+1} = \frac{4\psi_{i,N_y} - \psi_{i,N_y-1} - 3\psi_{i,N_y+1}}{2\Delta y} \tag{2.34}$$

For the present problem, the stream function at the boundaries is zero, and consequently, the velocities are given by:

$$v_{1,j} = \frac{\psi_{3,j} - 4\psi_{2,j}}{2\Delta x} \tag{2.35}$$

$$v_{N_x+1,j} = \frac{4\psi_{N_y,j} - \psi_{N_x-1,j}}{2\Delta x} \tag{2.36}$$

$$u_{i,1} = \frac{\psi_{i,3} - 4\psi_{i,2}}{2\Delta x} \tag{2.37}$$

$$u_{i,N_y+1} = \frac{4\psi_{i,N_y} - \psi_{i,N_y-1}}{2\Delta y} \tag{2.38}$$

2.4 Validation

The present numerical procedure was tested, using the numerical result obtained by Degan and Vasseur, (1996), for various Rayleigh numbers Ra, permeability ratio K^*, and anisotropic orientation angle θ. In this study, the aspect ratio is $A = 1$. The side walls of the cavity are heated and cooled isothermally, while the horizontal walls are adiabatic, the porous medium is anisotropic in permeability with its principal axes oriented in a direction that is oblique to the gravity vector, and the fluid density is linearly related to the temperature.

We only need to set the density inversion parameter $\gamma \to \infty$ to simulate the limiting case of a fluid with a linear equation of state. The following equation relates the linear Rayleigh number and non-linear Rayleigh number:

$$Ra_l = Ra(\gamma - 1) \approx Ra\gamma \tag{2.39}$$

where, Ra_l is the linear Rayleigh number.

In the comparison test, we used $\gamma = 10$ for most cases and 100 for some of them. The differences in Nusselt numbers and maximum stream functions are less than 2 percent when compared with the study of Degan and Vasseur, (1996).

Table 2.1 shows a comparison between the present results in term of Nusselt number with those of Degan and Vasseur, (1996), for different Rayleigh numbers, permeability ratios and orientation angles. A good agreement is observed between both results.

Table 2.1 The comparison with results of Degan and Vasseur, (1996)

Case	Rayleigh number Ra_l	Inversion parameter γ	Permeability ratio K^*	Orientation angle θ^o	Mesh size $x \times y$	Present method N_u	Degan results N_u
A	400	100	0.01	45	100 x 120	11.483	11.313
B	400	10	1	45	80 x 80	7.884	7.859
C	400	10	100	45	80 x 80	1.090	1.090
D	1	10	0.001	0	80 x 80	1.004	1.003
E	1	100	0.001	90	80 x 80	1.004	1.003
F	10000	100	100	0	100 x 120	9.741	9.967
G	10000	10	100	90	80 x 80	4.373	4.341

Figure 2.2 a-g illustrates the streamlines (left) and isothermal lines (right) for different conditions corresponding to the cases listed in Table 2.1. The inclined angle of the cavity is $\alpha = 90$ degree and aspect ratio is $A = 1$.

In order to obtain satisfying symmetry for all flow fields we had to increase the inversion parameter from 10 to 100 for case A, E and F. Those flow fields correspond quite closely to those of Degan's and Vasseur, (1996) for the same conditions.

Based on the comparison test above, the validity of the new numerical model and approach has been found satisfactory and will be used in the next chapter.

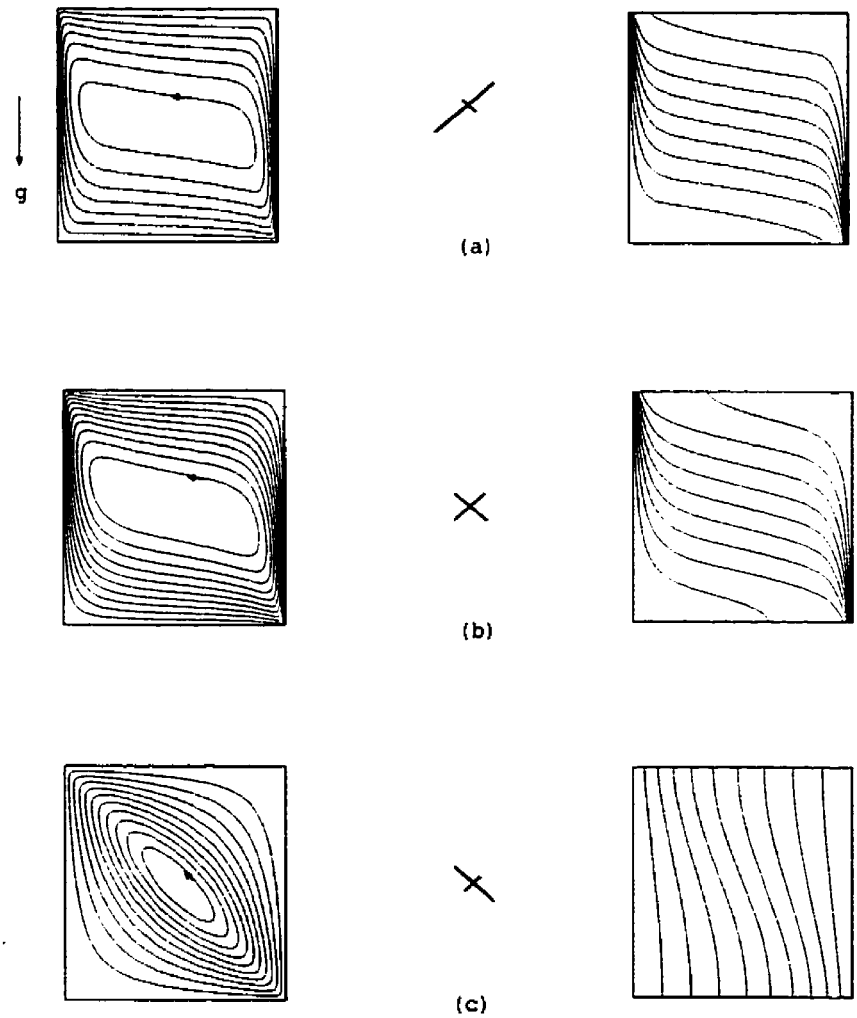

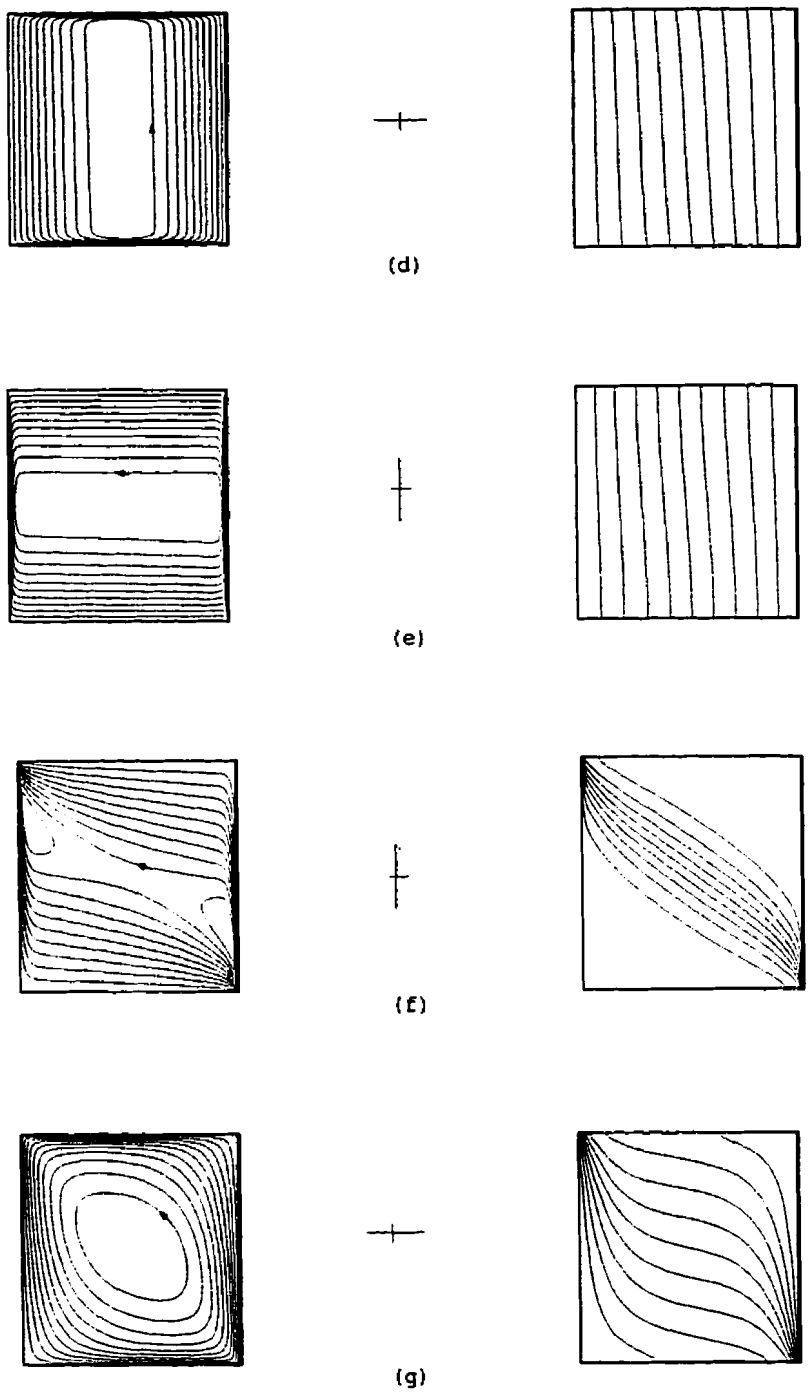

Figure 2.2 The comparison with results of Degan and Vasseur, (1996)

CHAPTER III.

RESULTS AND DISCUSSION

3.1 Effect of the inversion parameter γ (isotropic case)

As described among others in Robillard and Vasseur, (1991), convection in water involving the maximum density at 4 $^{\circ}C$ is characterized by the reduction of heat transfer and the doubling of convective cells when the maximum density lies within the flow domain. For the case of a rectangular cavity such as the one considered in the present study, the relative position, $x_m = A\ (\ 1-\gamma/2\ )$, of the pure conduction 4 $^{\circ}C$ isotherm with respect to the two vertical boundaries will strongly influence the convective heat transfer and the associated flow field. Figure 3.1 a-h, shows flow (left) and temperature (right) fields represented by streamlines and isotherms respectively for different values of γ. For $0<\gamma<2$, the 4 $^{\circ}C$ isotherm, shown by a heavy line in Figure 3.1 a-g, lies within the flow field. With γ increasing toward large values, the standard case of convection with linear density temperature relationship is recovered. For instance, Figure 3.1 h, with $\gamma=4$, represents qualitatively that type of free convection, the flow and temperature fields being almost symmetric with respect to the center of the cavity. The corresponding linear (or standard) Rayleigh number is $Ra_l = Ra_m(\gamma-1)=600$. In the sequence of flow fields shown in Figure 3.1 a-h, one may observe that the original clockwise cell (Figure 3.1 a) is gradually replaced by a counterclockwise cell which appears at right in Figure 3.1 b-c. With γ increasing, this cell is enhanced and eventually, a symmetric flow shown in Figure 3.1 d, is obtained when $\gamma=1$. With γ increasing further, the original clockwise cell is reduced in size and strength and is finally eliminated from the flow field (Figure 3.1 e-h). Such a behavior with changing γ has already been reported for the fluid case by Watson (1972), and Robillard and Vasseur (1979).

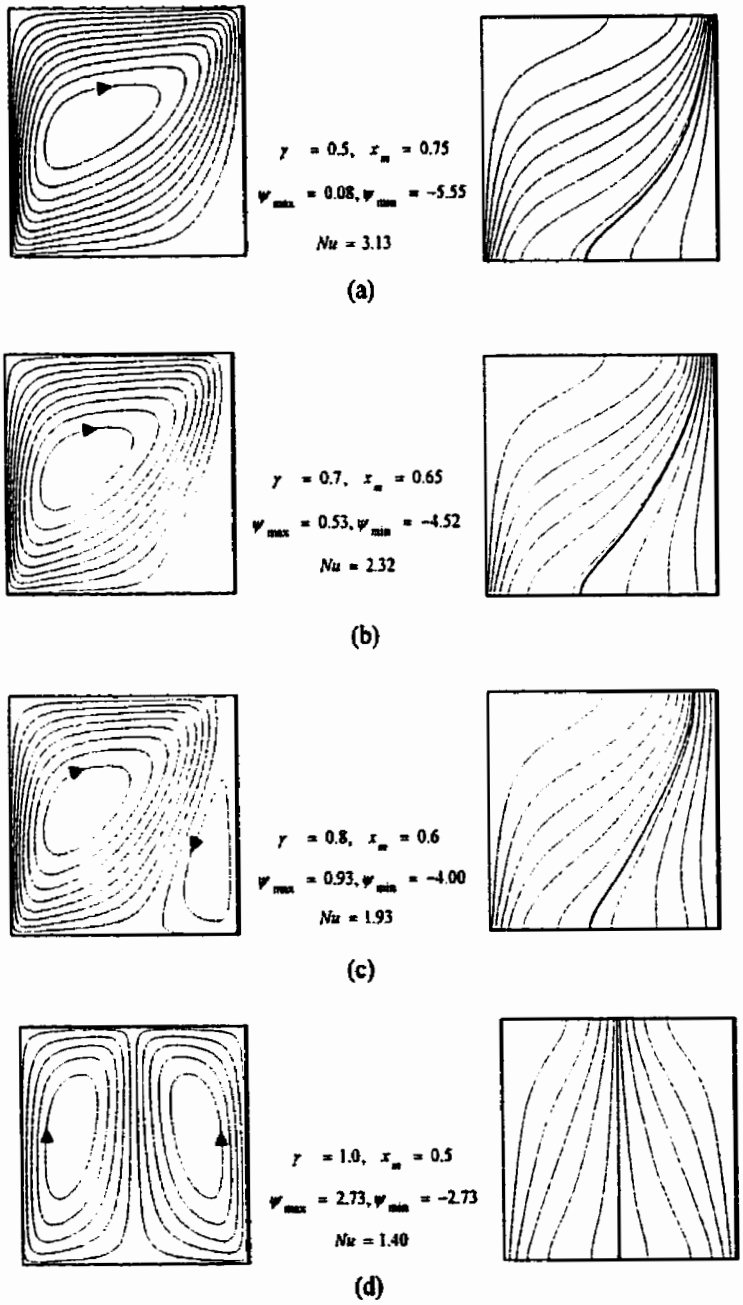

Figure 3.1 Flow and temperature fields at various γ,(Ra=200, K*=1, $\theta = 0$)

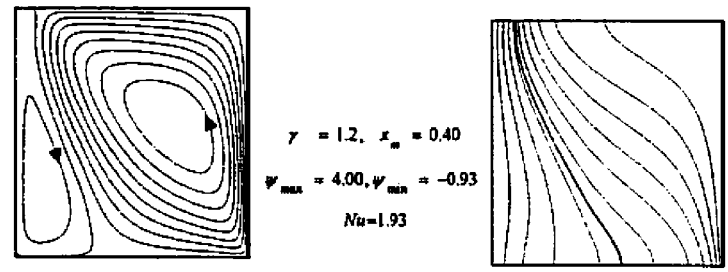

(e)

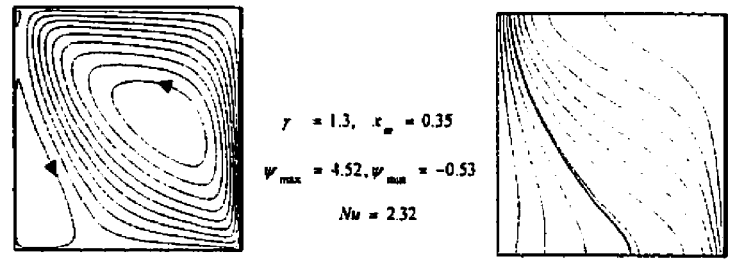

(f)

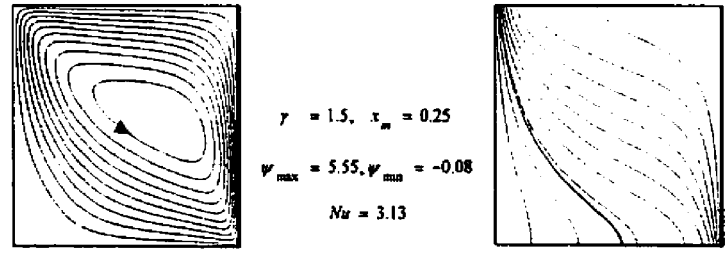

(g)

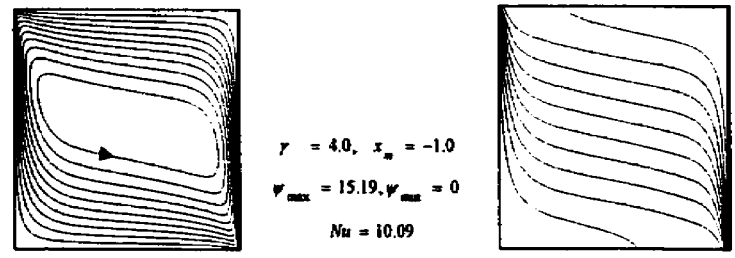

(h)

Figure 3.1 Flow and temperature fields at various γ ,(Ra=200, K*=1, $\theta = 0$)

The effect of γ on the Nusselt number is shown in Figure 3.2 for three different values of Ra_m, (25, 100 and 200). The Nusselt number reaches its minimum value at γ=1, value for which the left and right convective cells produce a symmetric flow field. It may also be noticed in Figure 3.2, that the curves are symmetric with respect to the vertical axis γ=1, i.e. the following relationship holds:

$$Nu(\gamma) = Nu(2-\gamma) \tag{3.1}$$

with corresponding flow fields being mirror images.

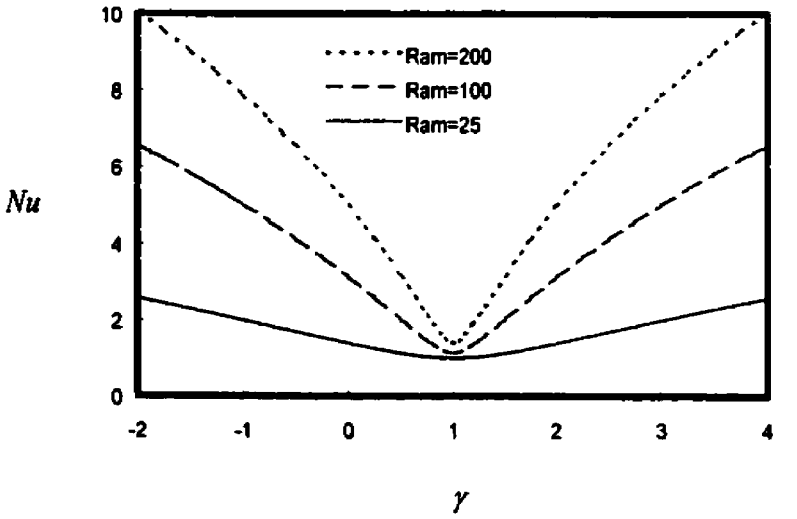

Figure 3.2 Nusselt number function of γ (isotropic case $Ra_m = 25, 100, 200$)

3.2 Effect of the permeability ratio K^* ($\gamma = 1;\ \theta = 0$)

As shown in Figure 3.1 d, a symmetric flow field with two counter-rotating convective cells is obtained for $\gamma = 1$ and $K^* = 1$. In order to isolate the effect of a change in permeability ratio K^* from the change in the overall hydraulic resistivity, (the hydraulic resistivity being the inverse of the permeability) we redefine the Rayleigh number in the following way. By considering the two hydraulic resistivities along the principal axes $R_1 = 1/K_1$ and $R_2 = 1/K_2$, we define an overall resistivity as

$$\overline{R} = R_1 + R_2 = \frac{1}{2}\frac{K_1 + K_2}{K_1 K_2} \tag{3.2}$$

and a modified Rayleigh number as

$$Ra_m = \frac{g\lambda\Delta T^2 H}{\nu\alpha}\frac{1}{\overline{R}} = Ra\left(\frac{2}{1+K^*}\right) \tag{3.3}$$

with the consequence that the extremum permeabilities K_1 and K_2 have the same weight in this new Rayleigh number.

Figure 3.3 shows the Nusselt number Nu, defined in Eq.(1.34), function of the permeability ratio K^* for different Rayleigh numbers ($Ra_m = 200$, 400, 600 and 800), the orientation angle θ being maintained at zero. Owing to the definition of Ra_m, the overall hydraulic resistivity remains constant along each curve of Figure 3.3. From the behavior of the curves in this figure, it is clear that a relative increase of the vertical permeability will enhance the heat transfer in the horizontal direction.

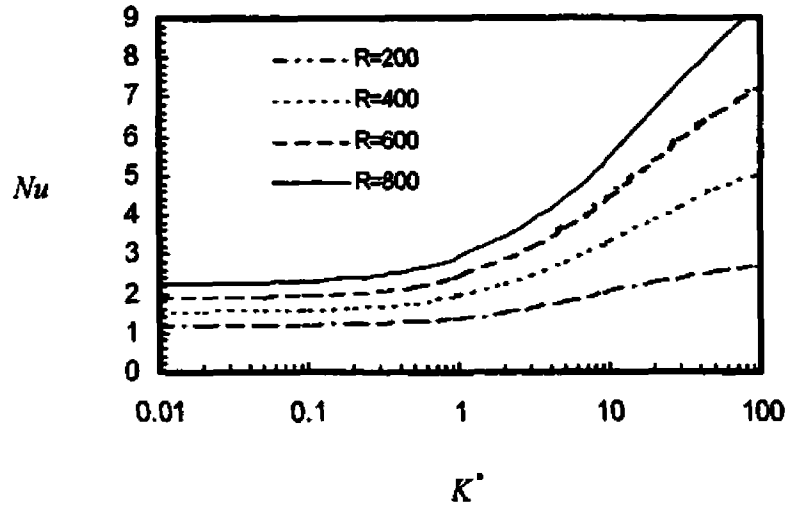

Figure 3.3 Nu function of K^* ($\theta = 0^o$, $\gamma = 1$, here, $R = Ra_m$)

The effect of K^* on the flow and temperature fields is shown in Figure 3.4 a,b,c,d when Ra_m=400, γ=1 and θ=0°. For each set of flow and temperature fields the relative importance of K_1 and K_2 is given by the relative length of the horizontal and vertical bars respectively, forming a cross between the flow field (left) and the temperature field (right). It is seen that the distortion of the isotherms is amplified with K^* increasing, the amount of distortion being related to the importance of convective heat transfer, $Nu - 1$. However for each of the flow and temperature fields shown in Figure 3.4, the symmetry with respect to a vertical line separating the cavity in two halves is preserved.

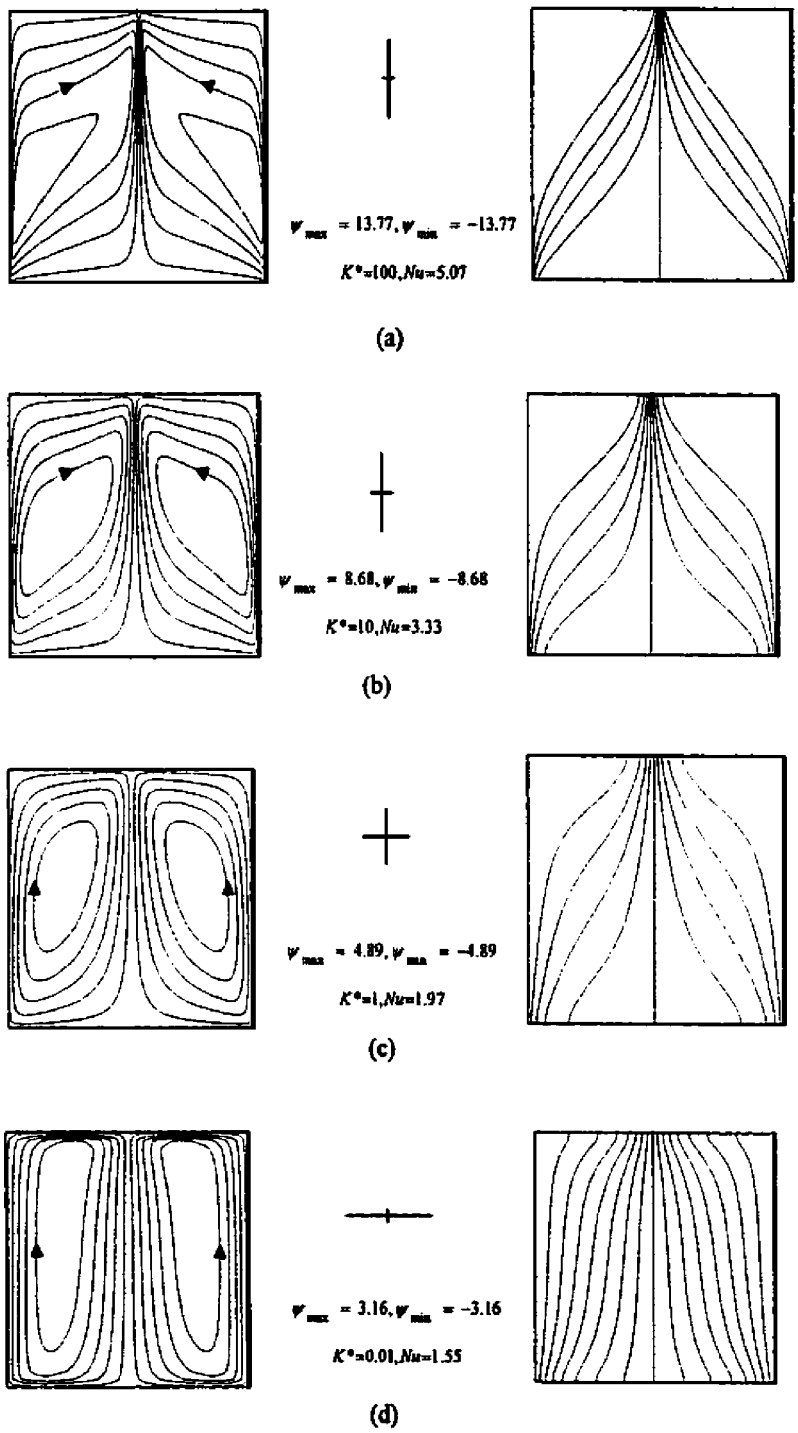

Figure 3.4. Flow and temperature fields at various K^*,($\gamma = 1$, $Ra_m = 400$, and $\theta = 0^o$)

3.3 Effect of the orientation angle θ

Figures 3.5 and 3.6 give the Nusselt number, Nu, and the extremum values of the stream function, ψ_{max} and ψ_{min}, as functions of the orientation angle θ. The extremum values ψ_{max} and ψ_{min} represent the intensities of the right and left convective cells respectively. In both Figures 3.5 and 3.6, three sets of curves are shown, corresponding to modified Rayleigh numbers, Ra_m, of 200, 400 and 800. For all those curves, γ and K^* are kept constant at respective values of 1 and 0.1. Flow and temperature fields corresponding to Ra_m=800 are shown in Figure 3.7 a-h for different values of θ from 0° to 90°. Other flow and temperature fields may be seen in Figure 3.8 a-e, for the same Ra_m and γ but for a stronger anisotropy, K^*=0.05. We may observe in Figure 3.5 the continuous transition for Nu from its minimum value to its maximum value, with θ increasing from 0° to 90°, i.e., with the maximum permeability axis being tilted from the horizontal to the vertical direction. In Figure 3.6, $|\psi_{min}|$ and ψ_{max} are seen to evolve from the minimum value $|\psi_{min}|=\psi_{max}$=6.03 at $\theta = 0^\circ$ to maximum value $|\psi_{min}|=\psi_{max}$=14.61 at $\theta = 90^\circ$. This equal intensity of the two conterrotating cells at 0° and 90° is a consequence of the symmetry described previously (part 3.2). However, for $0^\circ < \theta < 90^\circ$, this symmetry does not exist, as it can be observed in the sequences of flow and temperature fields of Figure 3.7 and Figure 3.8. With θ increasing from 0° to 90°, $|\psi_{min}|$ decreases at first to reach a minimum value of about 5.5 at $\theta \approx 13^\circ$, for the case Ra_m=800, whereas ψ_{max} increases continuously from 0° to 90°. Beyond $\theta \approx 13^\circ$, $|\psi_{min}|$ starts increasing faster than ψ_{max} and the equality $|\psi_{min}|=\psi_{max}$ is obtained at $\theta \approx 24^\circ$.

In the sequence of flow and temperature fields with a stronger anisotropy ($K^* = 0.05$, Figure 3.8), an interesting feature may be observed at $\theta = 22.5°$. The left convective cell shows two separate summits, which indicates a tendency for the cell to split into two separate convective cells.

The following trivial periodicity holds for an anisotropic porous medium:

$$\psi(\theta) = \psi(\theta \pm n\pi)$$

$$T(\theta) = T(\theta \pm n\pi) \tag{3.4}$$

where, $n = 1,2,\cdots$

Moreover, at $\gamma = 1$, the left and right cell intensities are related according to

$$\psi_{max}(\theta) = -\psi_{min}(\pi - \theta) \tag{3.5}$$

From Eq.(3.5), it is therefore possible to represent ψ_{min} and ψ_{max} as functions of θ, on a single curve such as the one given in Figure 3.9. One may notice in this figure that the maximum value ψ_{max} (or $\left| \psi_{min} \right|$) occurs when the maximum permeability axis is titled at an angle of about 8° with respect to the vertical direction and that the minimum value ψ_{max} (or $\left| \psi_{min} \right|$) occurs when the maximum permeability axis is titled at an angle of about 10° with respect to the horizontal direction.

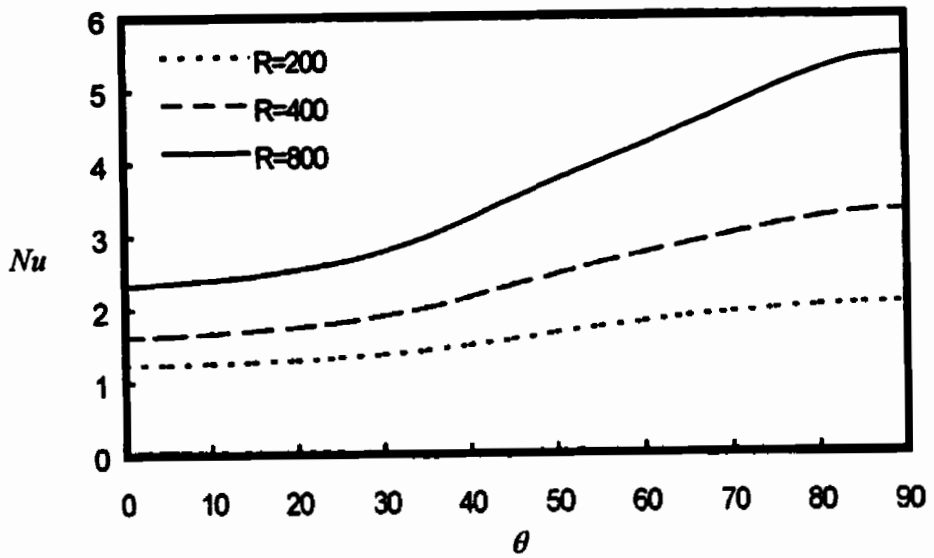

Figure 3.5. Nu function of θ, ($\gamma = 1$, $K^* = 0.1$)

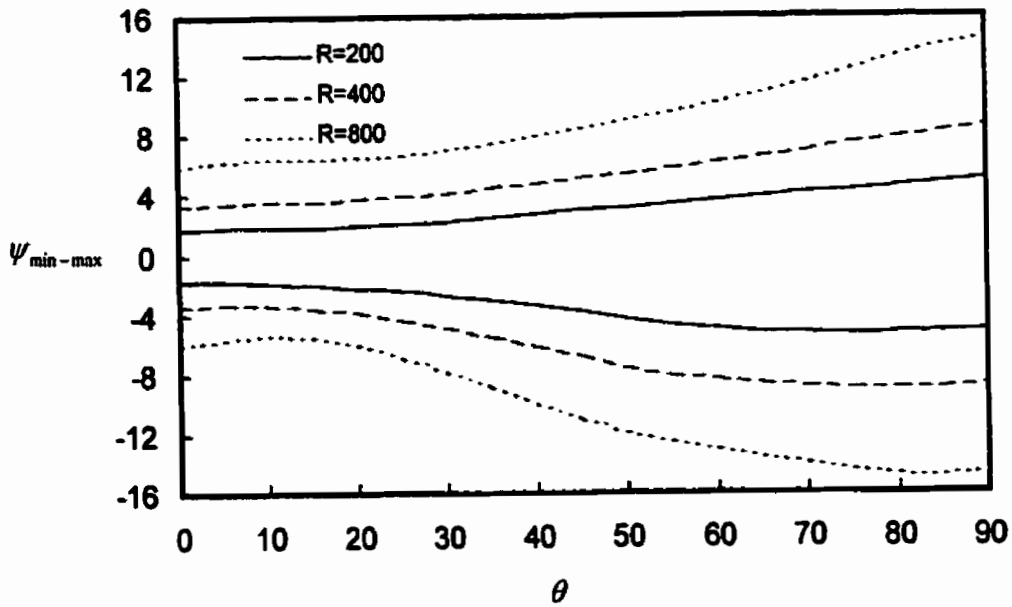

Figure 3.6. Extremum values ψ_{max} and ψ_{min} function of θ, ($\gamma = 1, K^* = 0.1$)

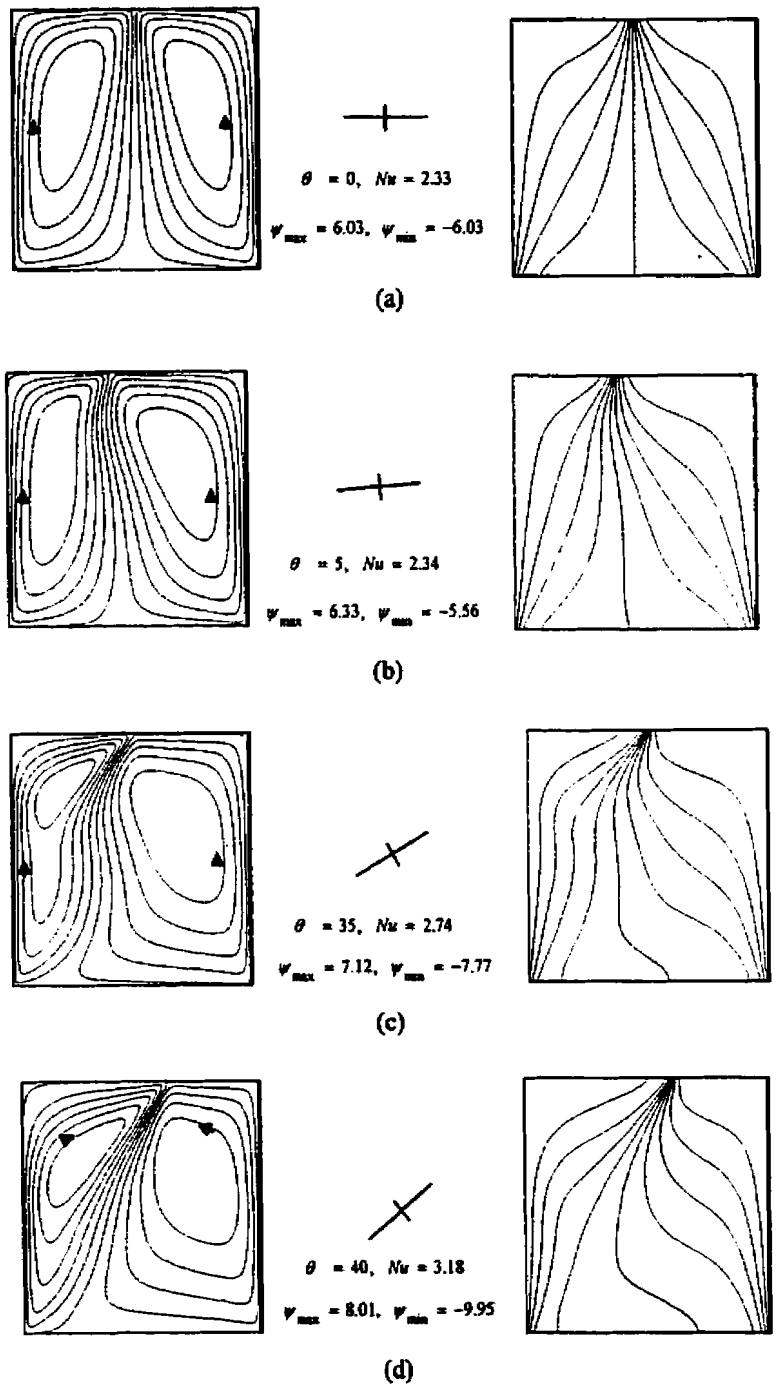

Figure 3.7. Flow and temperature fields at various θ, ($\gamma = 1$, $K^* = 0.1$, $Ra_m = 800$)

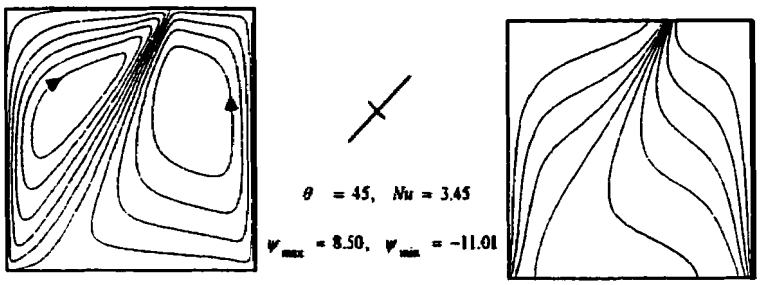

(e)

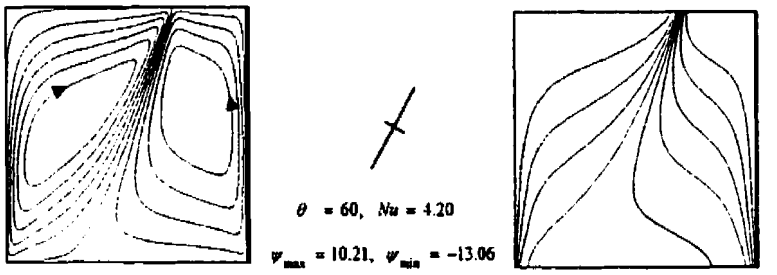

(f)

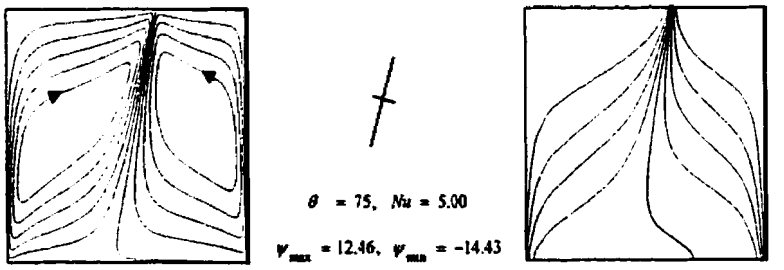

(g)

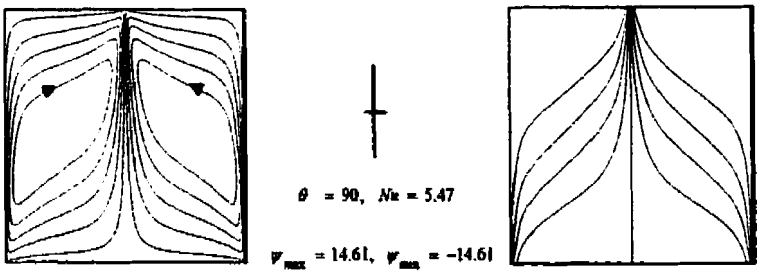

(h)

Figure 3.7. Flow and temperature fields at various θ, ($\gamma = 1$, $K^* = 0.1$, Ra_m=800)

(Continued)

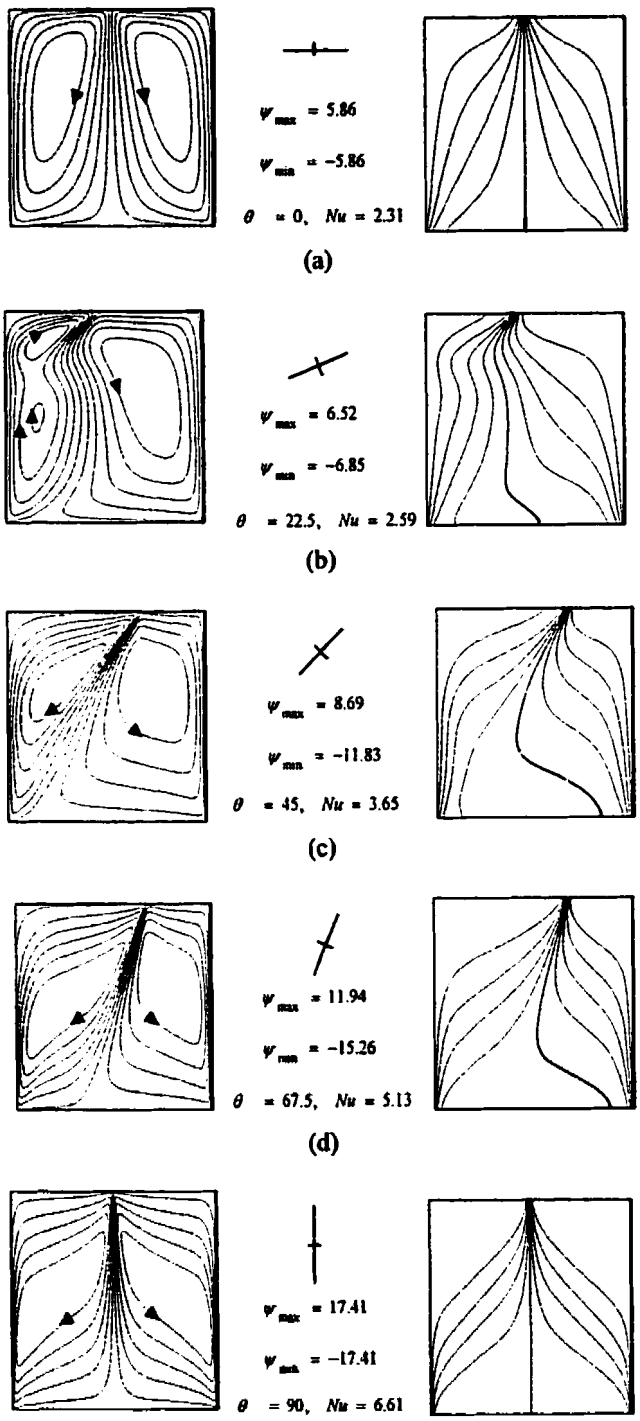

Figure 3.8. Flow and temperature fields at various θ, ($\gamma = 1$, $K^* = 0.05$, $Ra_m = 800$)

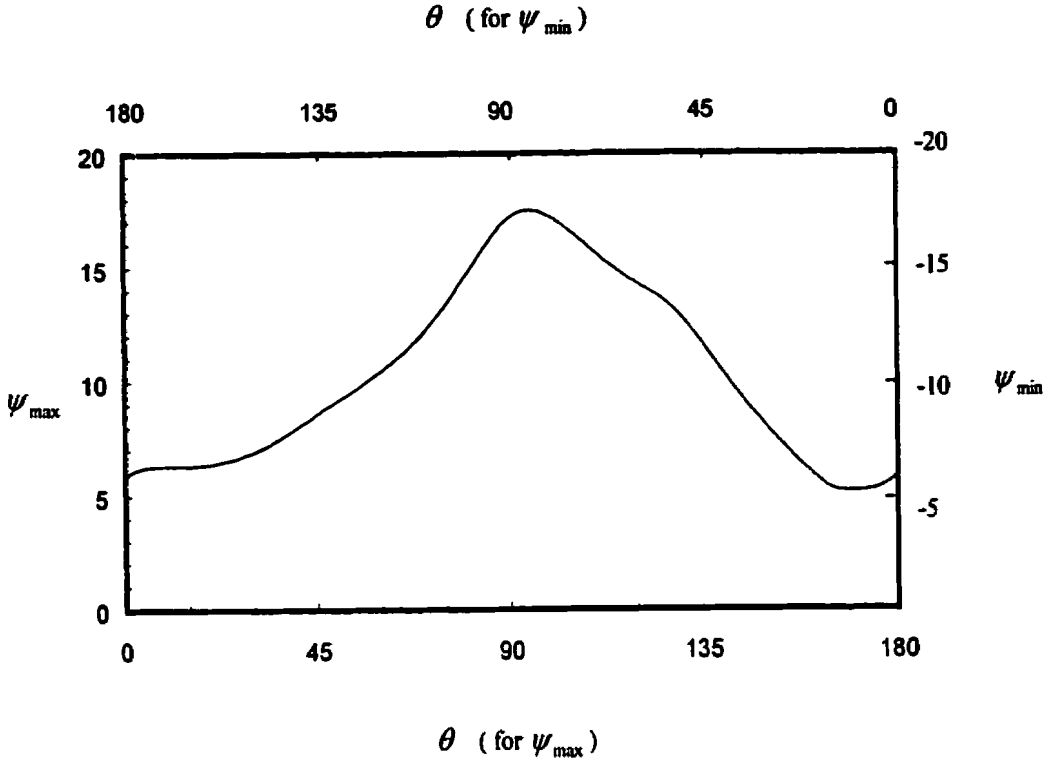

Figure 3.9. Extremum values ψ_{max} and ψ_{min} function of θ, ($\gamma = 1$, $K^* = 0.05$, $Ra_m = 800$)

3.4 Combined effect of γ and θ

It has been shown in Figure 3.2 that the Nusselt number reaches its minimum value at $\gamma = 1$ and that results are symmetric according to Eq. 3.1, for an isotropic porous medium. Moreover, at $\gamma = 1$ flow and temperature fields were found to be symmetric with respect to a vertical line separating the whole cavity in two equal parts (Figure 3.1d). This last symmetry of the flow and temperature fields holds for $K^* \neq 1$ (anisotropic medium) provided that $\theta = 0^o$, 90^o. Figures 3.10 a, b, 3.11 and 3.12 show the combined effect of γ and θ on the Nusselt number. In Figure 3.10 a, b, the Rayleigh number Ra_m and the permeability ratio have the respective values 100 and 0.05. Figure 3.10 b is an enlargement of Figure 3.10 a, with the range $0.8 \leq \gamma \leq 1.2$. Figure 3.11 shows the extended range $0 \leq \gamma \leq 10$ for Ra_m=25 and $K^* = 0.1$. This last figure reproduces results obtained by Degan and Vasseur, (1996), for the standard case of a linear density temperature relationship with $Ra_t = Ra_m(\gamma - 1)$. Figure 3.12 amplifies the convective effect on Nu in the neighborhood of $\gamma = 1$ with $Ra_m = 600$. It is clearly observed in Figure 3.10 b that the curves corresponding to $0^o < \theta < 90^o$ do not have the symmetry defined by Eq. 3.1. That loss of symmetry is much amplified in Figure 3.11 for all the curves for which $\theta \neq 0^o, 90^o$.

For the isotropic porous medium and also for the anisotropic case with $\theta = 0^o$, 90^o the minimum Nusselt number at $\gamma = 1$ corresponds to symmetric flow fields as shown in Figure 3.1 d, 3.7 a, 3.7 h, 3.8 a and 3.8 e, with $|\psi_{min}| = \psi_{max}$. Such a symmetry at minimum Nu does not exist anymore when $\theta \neq 0^o, 90^o$ for an anisotropic porous medium.

Figure 3.13 a, b shows the flow and temperature fields for $K^* = 0.05$, $Ra_m = 100$ and $\theta = 67.5°$, and for two different values of γ. Figure 3.13 a, corresponds to the minimum value of Nu obtained at $\gamma = 1.09$, with $|\psi_{min}| = 2.86$ and $\psi_{max} = 2.55$. Figure 3.13 b obtained at $\gamma = 1.12$ shows two cells with equal intensity $|\psi_{min}| = \psi_{max} \approx 2.56$.

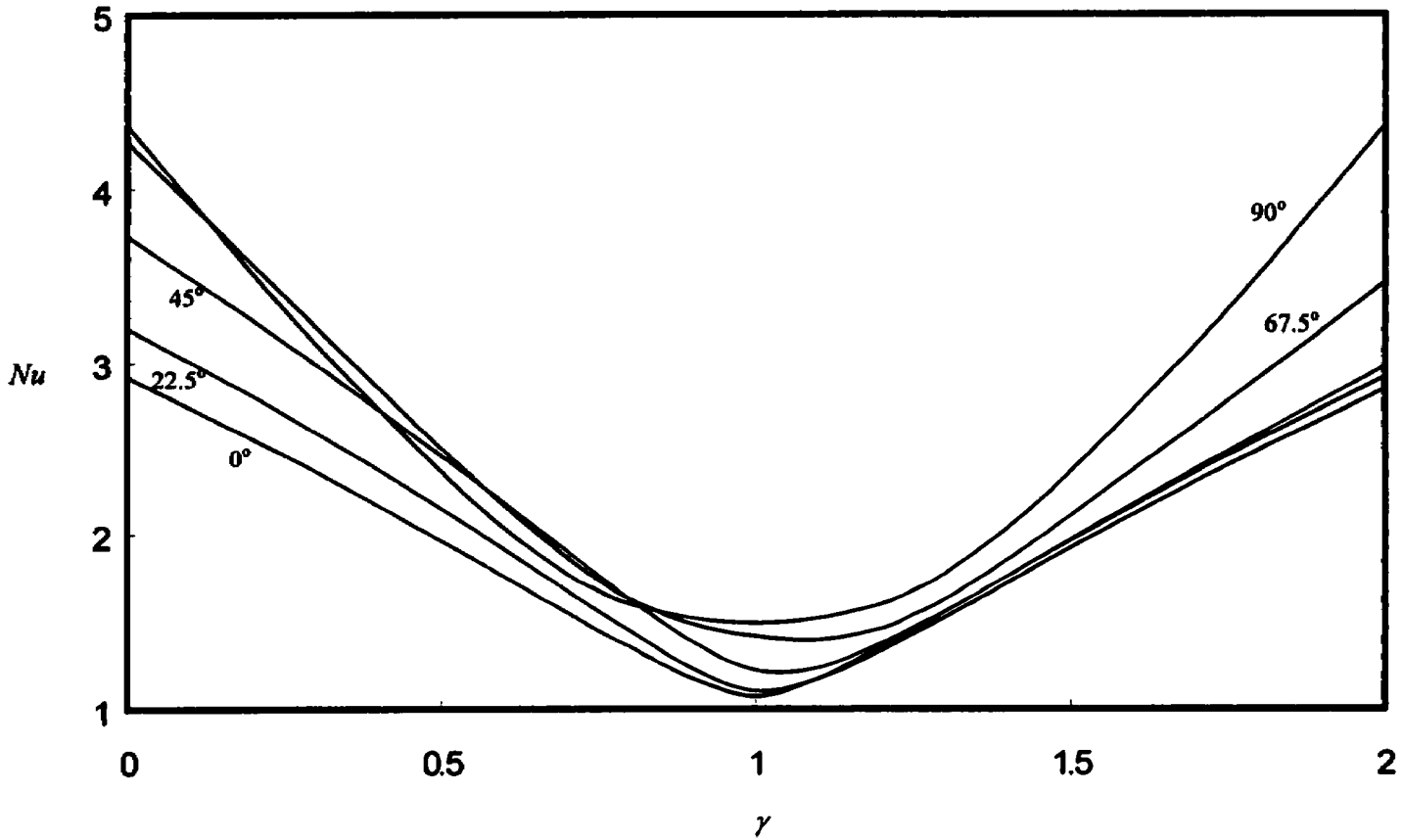

Figure 3.10 a. Nu function of γ at various θ (K^*=0.05, Ra_m=100)

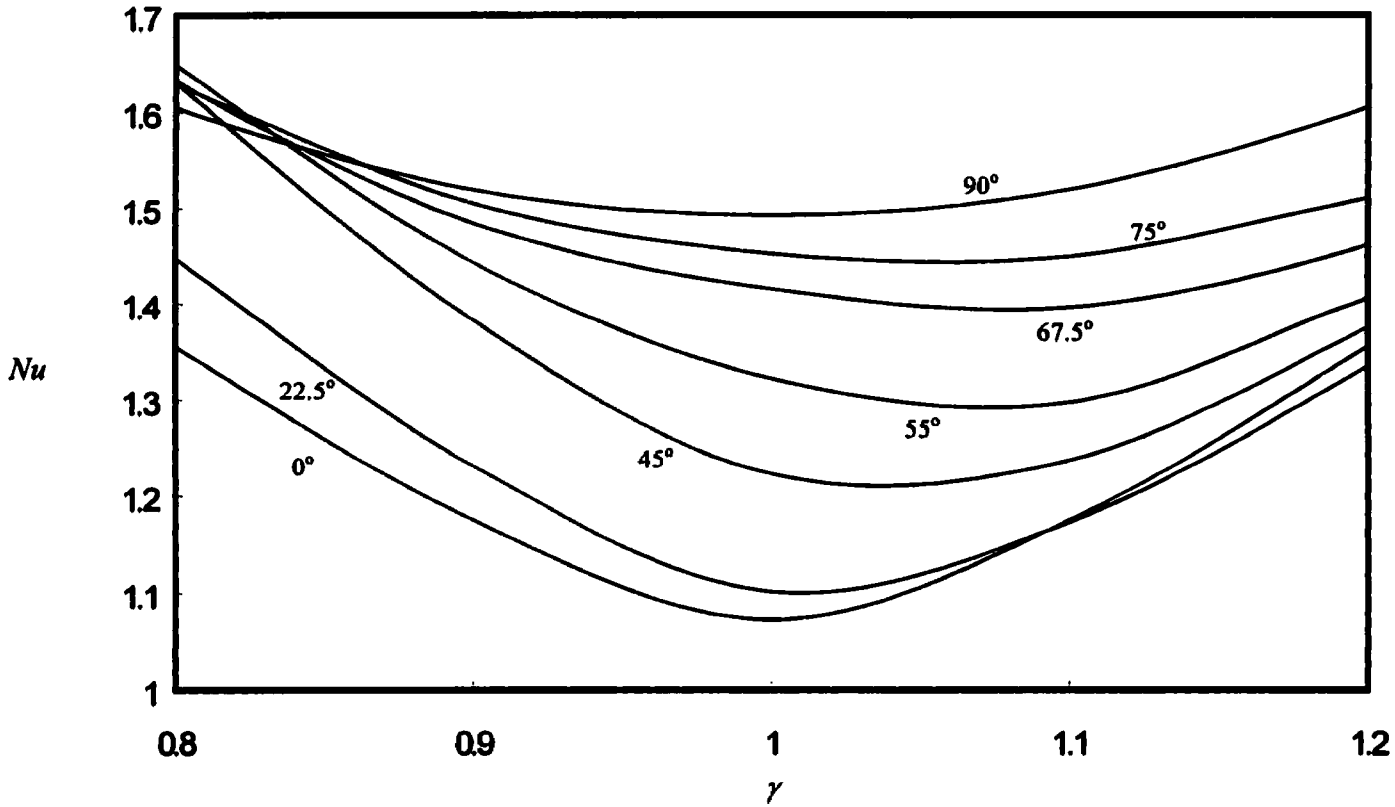

Figure 3.10 b. Nu function of γ at various θ (K^*=0.05, Ra_m=100)

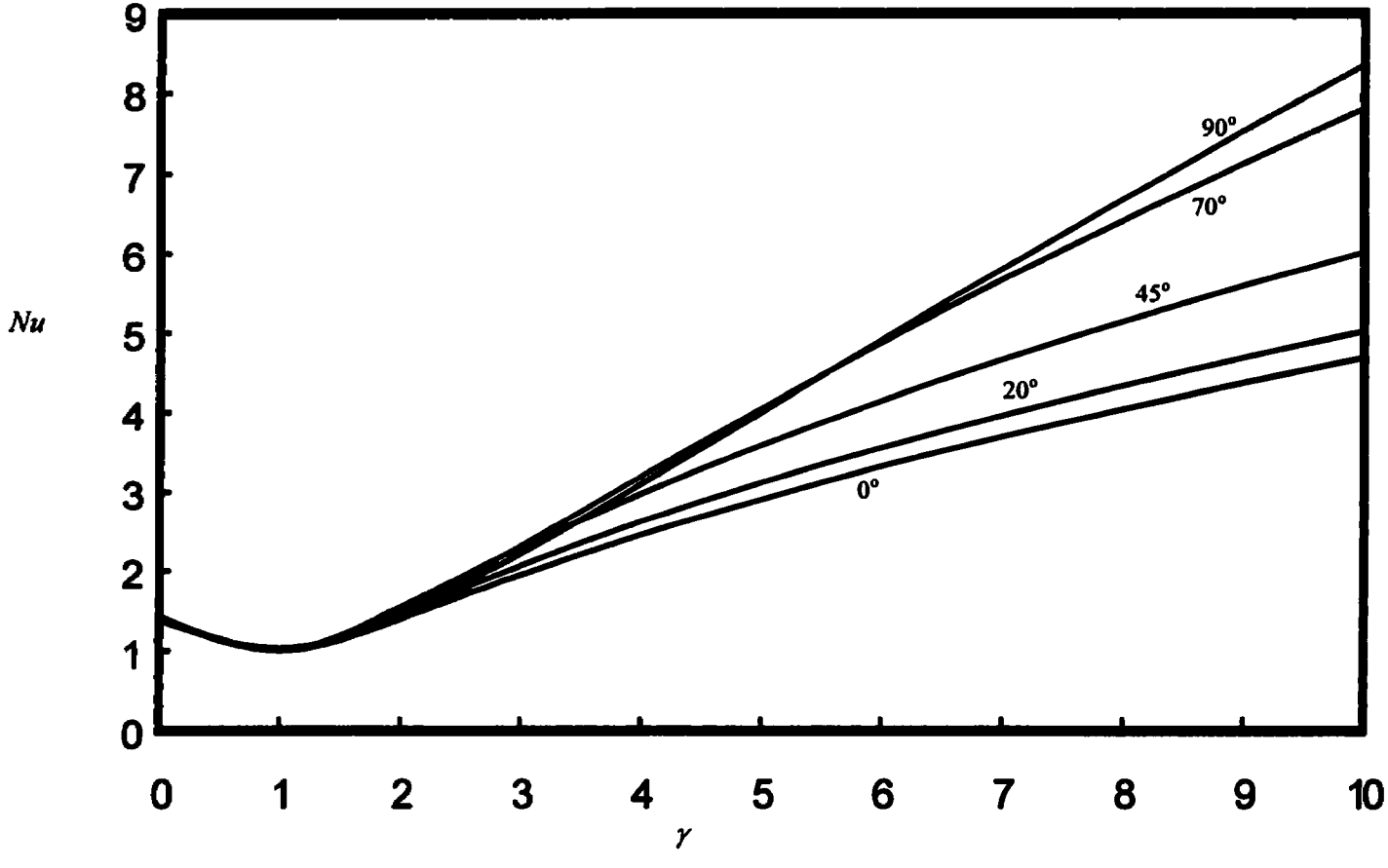

Figure 3.11. Nu function of γ at various θ (K^*=0.1, Ra_m=25)

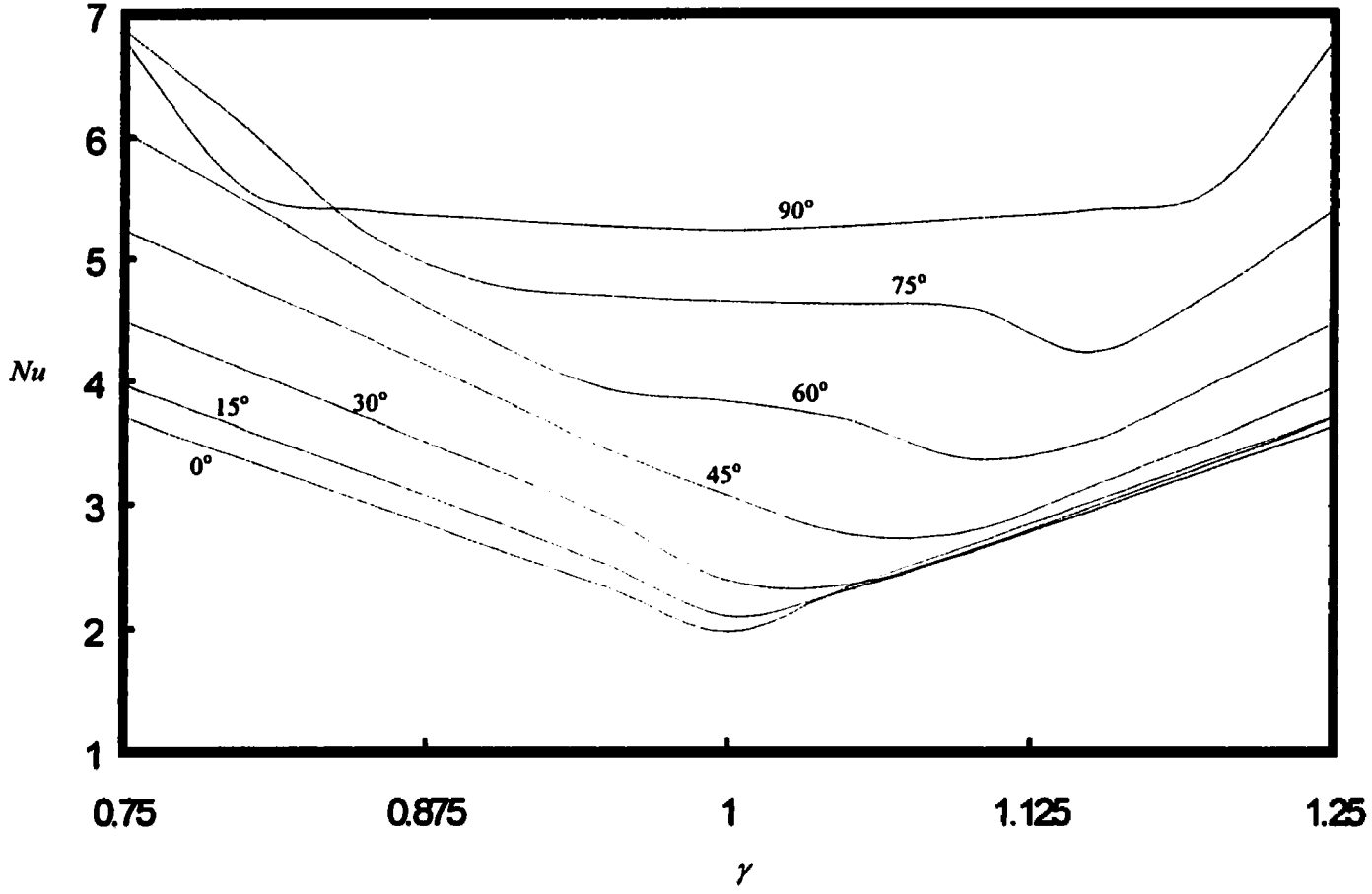

Figure 3.12 *Nu* function of γ at various θ (K^*=0.05, Ra_m=600)

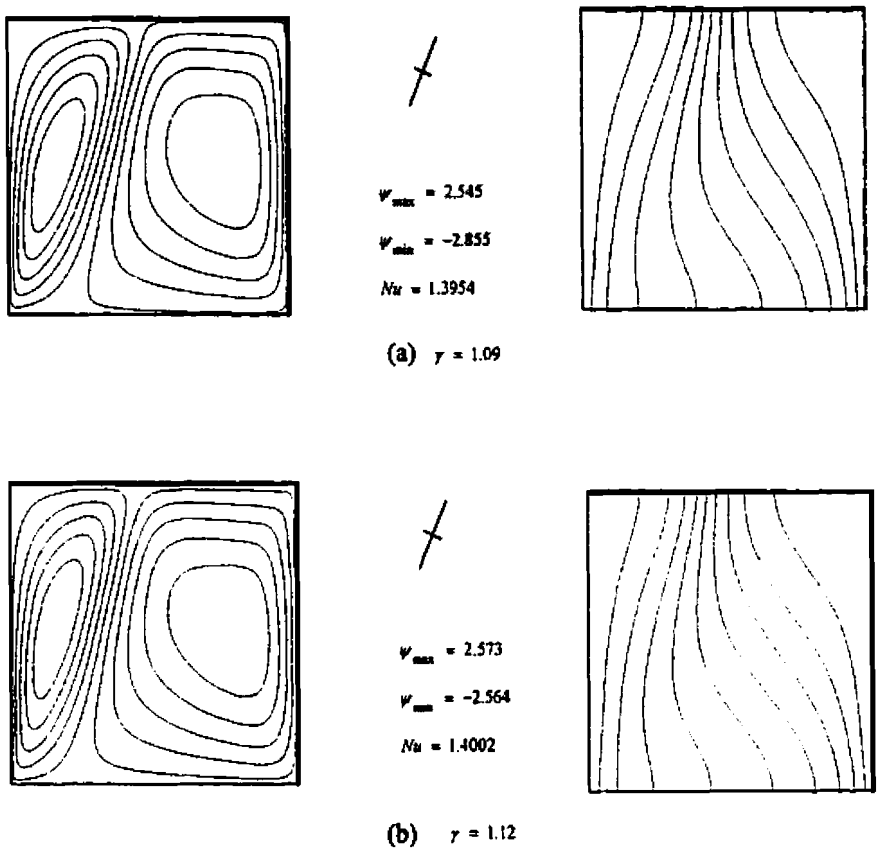

Figure 3.13 Flow and temperature fields at θ=67.5°, K^*=0.05 and Ra_m=100.

CONCLUSION

The effects of density inversion characterizing water near 4 ^{o}C have been investigated for the case of an anisotropic porous medium, saturated with water, contained in a square cavity and the two vertical side walls being maintained at uniform temperatures. A flow model based on the Darcy's law and Boussinesq approximation, and a numerical approach based on finite difference method have been developed to simulate the fluid flow and heat transfer. The flow model and the numerical approach developed in the present study have been validated by comparison with the results of Degan and Vasseur, (1996), done for anisotropy with linear relationship between density and temperature.

Numerical results were then obtained for the density inversion in water, by varying the anisotropic angle θ, the permeability ratio K^* and the inversion parameter γ, this last parameter being directly related to the horizontal position of the pure conduction maximum density with respect to the side walls.

Results with $\theta = 0^{o}$ and 90^{o} (horizontal/vertical principal axes) indicate that the maximum convection and heat transfer occur when the maximum permeability is in the vertical direction. With oblique axes ($\theta \neq 0^{o}$ or 90^{o}), it was found that the symmetry of flow and temperature fields observed for the isotropic porous medium at $\gamma = 1$ (value for which the temperatures of side walls are equidistant from the maximum density temperature of 4 ^{o}C) does not exist anymore for the anisotropic porous medium. Moreover, for those conditions, the minimum Nusselt number does not occur at $\gamma = 1$, but is shifted slightly above or below unity, at a value for which the symmetry of flow and temperature fields are not recovered.

Future studies should be undertaken to investigate the heating from below, since the finite amplitude convection in those condition implies the presence of a stable layer superposed to the unstable one with specific features such as penetrative convection and subcritical bifurcation.

REFERENCES

ABOUBI, K., ROBILLARD, L. and BILGEN, E. (1995). Convective Heat Transfer in Annular Porous Layer with Centrifugal Force Field. Numerical Heat Transfer, Part A, 28, 375-388.

ALAVYOON, F. (1993). On Natural Convection in Vertical Porous Enclosures Due to Prescribed Fluxes of Heat and Mass at the Vertical Boundaries, Int. J. Heat Mass Transfer, 36, 2479-2498.

ALTIMIR, I. (1984). Three-dimensional Free Heat Transfer in Saturated Porous Media with Maximum Density Effects, Int. J. Heat Mass Transfer, 27, No. 10, 813-1824.

BEAR, J. (1972). «Dynamics of Fluids in Porous Media», American Elsevier Publishing Company, Inc., New York.

BECK, L. J. (1972). Convection in a Box of Porous Material Saturated with Fluid, Phys. Fluids, 15, 1377-1388.

BEJAN, A. (1984). «Convection Heat Transfer», Wiley, New York.

BEJAN, A. (1983). The Boundary Layer Regime in a Porous Layer with Uniform Heat Flux From the Side, Int. J. Heat Mass Transfer, 26, 1339-1346.

BERA, P., ESWARAN, V. and SINGH, P. (1998). Numerical Study of Heat and Mass Transfer in an Anisotropic Porous Enclosure Due to Constant Heating and Cooling, Numerical Heat Transfer, Part A, 34, 887-905.

BLAKE, K. R., BEJAN, A. and POULIKAKOS, D. (1984). Natural Convection Near 4°C in a Water Saturated Porous Layer Heated From Below, Int. J. Heat Mass Transfer, 27, No. 12, 2355-2364.

BLAKE, K. R., POULIKAKOS, D. and BEJAN, A. (1984). Natural Convection Near 4°C in a Horizontal Water Layer Heated From Below, Phys. Fluids, 27, No. 11.

BURNS, P. J., CHOW, L. C. and TIEN, C. L. (1977). Convection in a Vertical Slot Filled with Porous Insulation, Int. J. Heat Mass Transfer, 29, 919-926.

CALTAGIRONE, J. P. (1975). Thermoconvective Instabilities in a Horizontal Porous Layer, J. Fluid Mech. 72, Part 2, 269-287.

CARNAHAN, B., LUTHER, H. A., and WILKES, J. O. (1969). «Applied Numerical Methods», John Wiley & Sons, Inc.

CHANG, W. J. and HSIAO, C. F. (1993). Natural Convection in a Vertical Cylinder Filled With Anisotropic Porous Media, Int. J. Heat Transfer, 36, 3361-3367.

CHANG, W. J. and LIU, H. C. (1994). Natural Convection in a Finite Wall Rectangular Cavity Filled with an Anisotropic Porous Medium, Int. J. Heat Mass Transfer, 37, 303-312.

CHANG, W. J. and YANG, D. F. (1995). Transient Natural Convection of Water Near its Density Extremum in a Rectangular Cavity Filled with Porous Medium, Numerical Heat Transfer, Part A, 28, 619-633.

CHEN, F., CHEN, C. F. and PEARLSTEIN, A. J. (1991). Convective Instability in Superposed Fluid and Anisotropic Porous Layers, Phys. Fluids A, 3, 556-565.

CHEN, F. and HSU, L. H. (1991). Onset of Thermal Convection in an Anisotropic and Inhomogeneous Porous Layer Underlaying a Fluid Layer, J. Appl. Phys., 69, 6289-6301.

CHENG, K. C., and SEKI, N. (1991). «Freezing and Melting Heat Transfer in Engineering», Hemisphere Publishing Corporation, New York.

COSTA, V. A. F. (1997). Double Diffusive Natural Convection in a Square Enclosure with Heat and Mass Diffusive Walls, Int. J. Heat Mass Transfer, 40, 4061-4071.

DEGAN, G., VASSEUR, P. and BILGEN, E. (1995). Convective Heat Transfer in a Vertical Anisotropic Porous Layer, Int. J. Heat Mass Transfer, 38, 1975-1987.

DEGAN, G. and VASSEUR, P. (1996). Natural Convection in a Vertical Slot Filled with an Anisotropic Porous Medium with Oblique Principal Axes, Numerical heat transfer, part A, 30, 397-412.

ENE, H. I. (1991). Effects of Anisotropy on the Free Convection From a Vertical Plate Embedded in a Porous Medium, Transport in Porous Media, 6, 183-194.

FARD, M. K., MOJTABI, M. C. C., and VAFAI, K. (1997). Non-Darcian Effects on Double-Diffusive Convection within a Porous Medium, Numerical Heat Transfer, Part A, 31, 837-852.

FATTAH, Q. N. and HOOPES, J. A. (1985). Dispersion in Anisotropic Homogeneous Porous Media, J. Hydraulic Engineering-ASCE, 111, 810-827.

HAN, H. and KUEHN, T. H. (1991). Double Diffusive Natural Convection in a Vertical Rectangular Enclosure – I. Experimental Study, Int. J. Heat Mass Transfer, 34, 449-459.

HAN, H. and KUEHN, T. H. (1991). Double Diffusive Natural Convection in a Vertical Rectangular Enclosure – II. Numerical Study, Int. J. Heat Mass Transfer, 34, 461-471.

HASNAOUI, M., VASSEUR, P., BILGEN, E. and ROBILLARD, L. (1995). Analytical and Numerical Study of Natural Convection Heat Transfer in a Vertical Porous Annulus, Chem. Eng. Comm., 131, 141-159.

HOWLE, L. E. and GEORGIADIS, J. G. (1994). Natural Convection in Porous Media with Anisotropic Dispersive Thermal Conductivity, Int. J. Heat Mass Transfer, 37, 1081-1094.

INABA, H. and FUKUDA, T. (1983). Natural Convection in an Inclined Square Cavity in Regions of Density Inversion of Water, J. Fluid Mech., 142, 363-381.

INABA, H. and FUKUDA, T. (1984). An Experimental Study of Natural Convection in an Inclined Rectangular Cavity Filled with Water at Its Density Extremum, Journal of Heat Transfer, 106, 109-115.

INGHAM, D. B. and POP, I. (1998). «Transport Phenomena In Porous Media», Pergamon.

KIMURA, S. and BEJAN, A. (1984). The Boundary Layer Natural Convection Regime in a Rectangular Cavity with Uniform Heat Flux From The Side, J. of Heat Transfer, 106, 98-103.

KIMURA, S., MASUDA, Y. and HAYASHI, K. (1993). Natural Convection in an Anisotropic Porous Medium Heated From The Side, Heat Transfer Japanese Research, 22, 139-153.

KVERNVOLD, O., and TYVAND, P. A. (1979). Nonlinear Thermal Convection in Anisotropic Porous Media, J. Fluid Mech., 90, 609-624.

LEGROS, J. C., LONGREE, D. and THOMAES, G. (1972). Benard Problem in Water Near 4 °C, Physics, 72, 410-414.

LIOU, J. H. and HONG, Z. C. (1998). Numerical Simulation of Double-Diffusive Natural Convection in a V-shaped Sump by a Control Volume Method Based on an Unstructured Triangular Grid, Numerical Heat Transfer, Part A, 34, 431-446.

MALASHETTY, M. S. (1993). Anisotropic Thermoconvective Effects on the Onset of Double Diffusive Convection in a Porous Medium, Int. J. Heat Mass Transfer, 36, No.9, 2397-2401.

MAMOU, M., VASSEUR, P. and BILGEN, E. (1995). Multiple Solutions For Double-Diffusive Convection in a Vertical Porous Enclosure, Int. J. Heat Mass Transfer, 38, 1787-1798.

MCKIBBIN, R. and TYVAND, P. A. (1982). Anisotropic Modelling of Thermal Convection in Multi-layered Porous Media, J. Fluid Mech., 118, 315-339.

MCKIBBIN, R. (1986). Thermal Convection in a Porous Layer: Effects of Anisotropy and Surface Boundary Conditions, Transport in porous media, 1, 271-292.

MERKER, G. P., WAAS, P. and GRIGULL, U. (1978). Onset of Convection in a Horizontal Water Layer with Maximum Density Effects, Int. J. Heat Mass Transfer, 22, 505-515.

MEYER, S., OSTROGORSKY, A. G. (1996). Forced Convection in Vertical Bridgman Configuration with the Submerged Heater, J. of Crystal Growth, 5539.

MOORE, D. R. and WEISS, N. O. (1973). Nonlinear Penetrative Convection, J. Fluid Mech., 61, Part 3, 553-581.

NGUYEN, H. D., PAIK, S. and DOGULASS, R. W. (1994). Study of Double-Diffusive Convection in Layered Anisotropic Porous Media, Numerical Heat Transfer, Part B, 26, 489-505.

NI, J. and BECKERMANN, C. (1991). Natural Convection in a Vertical Enclosure Filled with Anisotropic Porous Media, Trans. ASME: J. HEAT TRANSFER, 113, 1033-1037.

NIELD, D. A. and BEJAN, A. (1992). «Convection in Porous Media», Springer-Verlag, New York.

NILSEN, T. and STORESLETTEN, L. (1990). An Analytical Study on Natural Convection in Isotropic and Anisotropic Porous Channels, Trans ASME: J. Heat Transfer, 112, 396-401.

NISHIMURA, T., HAYASHIDA, Y. and MINEOKA, M. (1997). Oscillatory Natural Convection of Water Near the Density Extremum at High Rayleigh Numbers, Int. J. Heat Mass Transfer, 40, No. 14, 3449-3465.

PATANKAR, S. V. (1980). «Numerical Heat Transfer and Fluid Flow», Mc Graw Hill, New York.

POULIKAKOS, D. (1985). Onset of Convection in a Horizontal Porous Layer Saturated with Cold Water, Int. J. Heat Mass Transfer, 28, No. 10, 1899-1905.

QIN, Y. and KALONI, P. N. (1994). Convective Instabilities in an Anisotropic Porous Media, Studies in Applied Mathematics, 91, 189-204.

REES, D. A. S. and STORESLETTEN, L. (1995), The Effect of Anisotropic Permeability on Free Convective Boundary Layer Flow in Porous Media, Transport in Porous Media, 19, 79-92.

ROBILLARD, L. AND VASSEUR, P. (1991). Convective Flow Generated by a Pipe in a Semi-Infinite Porous Medium Saturated with Water in the Neighborhood of 4 °C, «Freezing and Melting Heat Transfer in Engineering», Edited by CHENG, K. C. and SEKI, N., Hemisphere Publishing Corporation, 315-338.

ROBILLARD, L. and VASSEUR, P. (1979), Effect du Maximum de Densité sur la Convection Libre de L'eau dans une Cavité Fermée, Canadian Journal of Civil Engineering, 6, No. 4, 481-493.

ROSENBERG, N. D. and SPERA, F. J. (1990). Role of Anisotropic and or Layered Permeability in Hydrothermal Convection, Geophysical Research Letters, 17, 235-238

ROSEBERG, N. D., SPERA, F. J. and HAYMON, R. M. (1993). The relationship Between Flow and Permeability Field in Seafloor Hydrothermal Systems, Earth and Planetary Science Letters, 116, 135-153.

ROY, S. (1972). Free Convection in Liquids Under Maximum Density Conditions, Indian J. Phys., 46, 245-249.

SEKI, N., FUKUSAKO, S. and INABA, H., SAPPORO (1978). Free Convective Heat Transfer with Density Inversion in a Confined Rectangular Vessel, Warme- und Stoffubertragung 11, 145-156.

SHEKAR, B. C. (1980), Numerical Study On Natural Convection Heat Transfer with Density Inversion of Water Between Two Horizontal Concentric Cylinders, Master Thesis Ecole Polytechnique de Montreal.

SIMPKINS, P. G. and BLYTHE, P. A. (1980). Convection in Porous Layer, Int. J. Heat Mass Transfer, 23, 881-887.

STORESLETTEN, L. (1998), Effects of Anisotropy on Convective Flow Through Porous Media, «Transport Phenomena in Porous Media», pp. 261-282, Editors: INCHAM, D. B. and POP, I., PERGAMON.

STORESLETTEN, L. (1993), Natural Convection in a Horizontal Porous Layer With Anisotropic Thermal Diffusisvity, Transport in Porous Media, 12, 19-29.

SUN, Z. S., TIEN, C. and YEN, Y. C. (1969). Thermal Instability of A Horizontal Layer of Liquid with Maximum Density, AIChE Journal, 15, No. 6, 910-915.

TIEN, C., YEN, Y. C. and DOTSON, J. W. (1972). Free Convective Heat Transfer in a Horizontal Layer of Liquid – The Effect of Density Inversion, Heat Transfer-Tulsa, AIChE Symposium Series, 68, No.118.

TONG, W. and KOSTER, J. N. (1994). Density Inversion Effect on Transient Natural Convection in a Rectangular Enclosure, Int. J. Heat Mass Transfer, 37, No. 6, 927-938.

TREVISAN, O. V. (1987). Mass and Heat Transfer by High Rayleigh Number Convection in a Porous Medium Heated From Below, Int. J. Heat Mass Transfer, 30, 2341-2356.

TREVISAN, O. V. and BEJAN, A. (1985). Natural Convection with Combined Heat and Mass Transfer Buoyancy Effects in a Porous Medium, Int. J. Heat Mass Transfer, 28, 1597-1611.

TREVISAN, O. V. and BEJAN, A. (1985), Mass and Heat Transfer by Natural Convection in a Vertical Slot filled with Porous Medium, Int. J. Heat Mass Transfer, 29, 403-415.

TREVISAN, O. V. and BEJAN, A. (1987). Combined Heat and Mass Transfer by Natural Convection in a Vertical Enclosure, J. of Heat Transfer, 109, 104-112.

TREW, M. and MCKIBBIN, R. (1994). Convection in Anisotropic Inclined Porous Layers, Transport in Porous Media, 17, 271-283.

TYVAND, P. A. and STORELETTEN, L. (1991). Onset of Convection in Anisotropic Porous Medium With Oblique Principal Axes, J. Fluid Mech., 226, 371-382.

VASSEUR, P. and ROBILLARD, L. (1980). Transient Natural Convection Heat Transfer in a Mass of Water Cooled Through 4 °C, Int. J. of Heat and Mass Transfer, 23, No. 9, 1995-1205.

VASSEUR, P., ROBILLARD, L. and SHEKAR, B. C. (1981). A Numerical Study on Natural Convection Heat Transfer with Density Inversion of Water within a Horizontal Cylindrical Annulus, Research Report, Ecole Polytechnique de Montreal.

VASSEUR, P., SATISH, M. G. and ROBILLARD, L. (1987). Natural Convection in a Thin, Inclined Porous Layer Exposed to a Constant Heat Flux, Int. J. Heat Mass Transfer, 30, No.3, 537-549.

WANG, X. and ROBILLARD, L. (1995). Mixed Convection in an Inclined Channel With Localized Heat Sources, Numerical Heat Transfer, Part A, 28, 355-373.

WEBER, J. E. (1975). The Boundary Layer Regime for Convection in a Vertical Porous Layer, Int. J. Heat Mass Transfer,18, 569-573.

YEN, Y. C. (1974). Effects of Density Inversion on Free Convective Heat Transfer in Porous Layer Heated From Below, Int. J. Heat Mass Transfer, 17, 1349-1356.

WATSON, A. (1972). The Effect of the Inversion Temperature on the Convection of Water in an Enclosed Rectangular Cavity, Quart. Journ. Mech. And Applied Math., Vol. XXV, Pt.4, 1972.

ZHANG, X., NGUYEN, T. H. and KAHAWITA, R. (1993). Convective Flow and Heat Transfer in an Anisotropic Porous Layer With Principal Axes Non-coincident With The Gravity Vector, ASME HTD, 264, 79-86.